PHARMACIA

Pharmacia 69(3): 595–614
DOI 10.3897/pharmacia.69.e86504

Research Article

Synthesis, docking study, and structure-activity relationship of novel niflumic acid derivatives acting as anticancer agents by inhibiting VEGFR or EGFR tyrosine kinase activities

Yahya Yaseen[1], Ammar Kubba[2], Wurood Shihab[3], Lubna Tahtamouni[4,5]

1 *Department of Pharmaceutical Chemistry, College of Pharmacy, University of Tikrit, Tikrit, Iraq*
2 *Department of Pharmaceutical Chemistry, College of Pharmacy, University of Baghdad, Bagdad, Iraq*
3 *Department of Pharmaceutical Chemistry, College of Pharmacy, Ashur university college, Bagdad, Iraq*
4 *Department of Biology and Biotechnology, Faculty of Science, The Hashemite University, Zarqa, Jordan*
5 *Department of Biochemistry and Molecular Biology, College of Natural Sciences, Colorado State University, Fort Collins, Colorado, USA*

Corresponding author: Ammar Kubba (kubbaammar1963@gmail.com)

Received 12 May 2022 ♦ **Accepted** 27 May 2022 ♦ **Published** 5 July 2022

Citation: Yaseen Y, Kubba A, Shihab W, Tahtamouni L (2022) Synthesis, docking study, and structure-activity relationship of novel niflumic acid derivatives acting as anticancer agents by inhibiting VEGFR or EGFR tyrosine kinase activities Pharmacia 69(3): 595–614. https://doi.org/10.3897/pharmacia.69.e86504

Abstract

A new series of niflumic acid (NF) derivatives were synthesized by esterification of (NF) to give ester compound **1,** which was treated with hydrazine hydrate to produce (NF) hydrazide **2.** Hydrazine-1-carboxamide compounds (**3A–C**), and hydrazine-1-carbothioamide derivatives (**4A–D**) were synthesized by treatment of (NF) hydrazide with phenyl isocyanate, and phenyl isothiocyanate derivatives, respectively. The cyclization of (4B–D) and (3B) was achieved using NaOH solution to produce 1,2,4-triazole derivatives (**5A–C)** and **6**, respectively. The prepared compounds were characterized using IR, ^{1}HNMR, ^{13}CNMR, and MS (ESI) spectroscopy. A molecular docking study was performed to evaluate the binding affinity of the synthesized compounds against EGFR and VEGFR kinase domains which revealed that compounds **3B,** and **4A** had the best binding energy (-7.87, and -7.33 kcal/mol, respectively) against VEGFR, while compound **5A** had the best binding energy (-7.95 kcal/mol) against EGFR. The biological investigation results indicated that all the tested compounds caused cell killing in the two cancer cell lines (Hep G2 and A549) studied, with compound **4C** being the most cytotoxic, as well as being cancer selective. Additionally, compound **4C**-treated Hep G2 cells were arrested at the S and G2/M cell cycle phases. Cytotoxicity of compound **4C** was attributed to apoptosis as determined by flow cytometry and qRT-PCR results of the apoptosis markers p53, BAX, and caspase-3. Finally, compound **4C** inhibited VEGFR kinase activity, while compound **5B** inhibited EGFR kinase activity. In conclusion, the novel (NF) derivatives are potent anticancer agents, inhibiting cell proliferation by inhibiting EGFR and VEGFR tyrosine kinase enzymes.

Keywords

ADMET, Apoptosis, EGFR kinase activity, MTT assay, 1,2,4 Triazole, VEGFR kinase activity.

Copyright *Yaseen Y et al.* This is an open access article distributed under the terms of the Creative Commons Attribution License (CC-BY 4.0), which permits unrestricted use, distribution, and reproduction in any medium, provided the original author and source are credited.

PENSOFT

Introduction

Cancer is a malignant illness in which cancer cells divide aberrantly without control, and it has been one of the world's biggest health issues for decades. Cancer affects a wide population of people around the world, and if not treated appropriately, it can cause invasion into the surrounding tissue, spread to other regions of the body, and become a significant health problem (Husain et al. 2012; Mirza et al. 2019). Every year, more than 11 million people are diagnosed with cancer, with an estimated 16 million new cases by the end of 2020 (Bhatt et al. 2010; Rashid et al. 2012).

Angiogenesis control is one of the main focuses for cancer therapy. One key aspect of the angiogenesis therapy is targeting the vascular endothelial growth factor (VEGF), whose family consists of five related glycoproteins (Pandey et al. 2018). Binding of VEGF to its receptors, VEGFR1 and VEGFR2, on the surface of endothelial cells, causes an increase in intracellular calcium and the production of vasodilator mediators, such as nitric oxide (Shibuya 2011; Pandey et al. 2018). In both normal physiological and pathological conditions, VEGF plays an important role in the development, progression, and formation of new blood vessels, as well as vascular leakage (Rubio and Adamis 2015; Amadio et al. 2016). Therefore, blockage of VEGF activity has become one of the main strategies in the treatment of cancer.

On the other hand, certain types of cancer are treated using epidermal growth factor receptor (EGFR) tyrosine kinase inhibitors. EGFR is found on the surface of normal cells and aids in cell development. However, the highest concentration of EGFR is found in malignant cells, which aids in their growth and division. As a result, inhibiting EGFR will halt cancer cell proliferation (Seshacharyulu et al. 2012). The EGFR kinase receptor protein belongs to the ErbB receptor family, and it mediates its activity by forming a heterodimer with other members of this family of receptors. This dimerization induces intrinsic protein-tyrosine kinase activity, which results in autophosphorylation of its C-terminal tyrosine residues. The auto-phosphorylation in turn results in induction of signaling cascades, such as AKT, mitogen-activated protein kinase, as well as the JNK pathway, which ultimately results in synthesis of DNA, cell cycle progression, and cell proliferation (Yarden and Schlessinger 1987; Oda et al. 2005).

The chemical properties of 1,2,4-triazoles, and their heterocyclic fusion derivatives have attracted great interest in recent decades, due to their various biological effects (Al et al. 2020). An increasing number of ring systems with 1,2,4-triazoles have been found to be used in different therapeutic drug candidates, including central nervous system drugs, anti-inflammatory, antimicrobial, and sedative agents (Heindel and Reid 1980; Shaker 2006). Their antimycotic activities are evident in their use in voriconazole, itraconazole, and fluconazole (Holla et al. 1994). Having antimitotic effects, triazole derivatives possess a wide range of applications in both medicine and agriculture (Bulut et al. 2018). The current research aimed to synthesize new niflumic acid derivatives which, through docking studies, were predicted to act as VEGFR-2 kinase inhibitors. The novel NF derivatives containing 1,2,4-triazole were synthesized and chemically characterized, and they were evaluated *in vitro* for their anticancer activities.

Experimental part

Materials and methods

Niflumic acid was purchased from Sigma-Aldrich. The infrared spectra were recorded using Shimadzu Specac GS 10800-R IR Affnity-1 Spectrophotometer (ύ = cm^{-1}). The mass spectra were recorded on Api 3200 triple quadruple, ESI system (Applied Biosystem). ^{1}HNMR spectra of the synthesized compounds were measured on AVANCE-III 300MHz Nanobay FT-NMR spectrometer, using tetramethylsilane (TMS), as an internal standard, the chemical shift was displayed once as (δ, ppm), and $DMSO_{d6}$ was utilized as a solvent.

Synthesis of ethyl 2-((3-(trifluoromethyl) phenyl) amino) nicotinate (1) (Al-Bayati et al. 2021)

A suspension of niflumic acid (0.035 mol, 10 g) in 85 mL abs. EtOH was cooled down to -15 °C, then an excess amount of thionyl chloride ($SOCl_2$) was added drop by drop (0.035 mol, 10.28 mL, 4.21 g). The temperature was kept below -10 °C. The reaction mixture was kept at a temperature of 40 °C for 3 h on a magnetic stirrer, then it was refluxed for 48 h, and left at RT overnight. The solvent was evaporated to dryness, then re-dissolved in abs. EtOH, and evaporated once more. The process was repeated to make sure that all excess $SOCl_2$ was removed. The product was then washed with 10% NaOH. The residue was collected and recrystallized from 70% EtOH.

Brown powder, yield (55%), m.p = 65–68 °C, R_f = 0.47. ATR-FTIR (ύ, cm^{-1}): 3264 (NH) str, 2925, 2858 (CH) str. of *aliph* (CH_2) and (CH_3), 1689 (C = O) str. of (conj ester), 1620 (C = N) str, 1582, 1534, 1498Ar (C = C) str.1403 (C-F) str, 1290 (C-N) str.

^{1}H-NMR (300MHz, $DMSO_{d6}$, δ = ppm): 10.29 (s, 1H, NH), 8.45–8.28 (m, 3H, Ar-H), 7.85 (d, 1H, Ar-H), 7.52–7.33 (d, 2H, Ar-H), 6.95 (s, 1H, Ar H), 4.36 (q, 2H, CH_2), 1.27 (t, 3H, Ar-H).

^{13}CNMR (75MHz, $DMSO_{d6}$, δ = ppm): 166.80 (C = O), 154.88 (ArC = N), 152.96, 140.56, 140.42, 129.90, 123.76 (CF_3), 118.57, 115.97, 114.99, 107.93, 61.56 (CH_2), 14.11 (CH_3).

MS (ESI) m/z: Calcd. for $C_{15}H_{13}F_3N_2O_2$ $[M]^+$ 310.09, found 310.90

Synthesis of 2-((3-(trifluoromethyl) phenyl) amino) nicotinohydrazide (2) (Hmood et al. 2021)

Niflumic ethyl ester (**compound 1**) (0.008 mol, 2.5 g), and hydrazine hydrate 80% (an excess amount of 0.0215 mol, 0.25 g, 5 mL) was added to 50 mL of EtOH in a 100 mL R.B flask, and the mixture was stirred overnight at RT, then it was set to reflux at 80 °C for 14 h. At the end of the reflux time, the mixture was stirred overnight at RT. Later, the mixture was then poured on crushed ice. The formed ppt was filtered off, and washed thoroughly with cold D.W. Then the ppt was allowed to dry, until being recrystallized from abs. EtOH.

White powder, yield (80%), m.p = 139–142 °C, R_f = 0.17. ATR-FTIR (ύ, cm^{-1}): 3306, 3205 (NH_2) str of *prim* amine , 1603 (C = O) str. of amide (amide I band), 1534, and 1445 Ar (C = C) str , 1400 (C-F) str, 1338 (C-N) str.

^{1}HNMR (300MHz, $DMSO_{d6}$, δ = ppm): 11.03 (s, 1H, NH), 10.13 (s, 1H, NH), 8.37–8.30 (d, 2H, Ar-H), 8.08 (s, 1H, Ar-H), 7.81, (d, 1H, Ar-H), 7.53 (t, 1H, Ar-H), 7.29 (d, 1H, Ar-H), 6.93(d,1H,Ar-H), 4.65 (s, 2H, NH_2).

^{13}CNMR (75MHz, $DMSO_{d6}$,δ = ppm): 166.63 (C = O), 153.91 (ArC = N), 150.38, 141.17, 136.60, 129.95, 122.77 (CF_3), 117.66, 114.87, 114.56, 111.17.

MS (ESI) m/z: Calcd. for $C_{13}H_{11}F_3N_4O$ $[M]^+$ 296.09, found 296.8.

General method for synthesis of niflumic hydrazine- carboamide derivatives (3A, 3B, and 3C) (Nederlof 1963)

To a solution of compound (**2**) (0.00084 mol, 0.25 g,) in 25 mL of EtOH was added separately, (A): 1-bromo-4-isocyanatobenzene (0.00084 mol, 0.18 g), (B): 1-chloro-4-isocyanatobenzene (0.00084 mol, 0.14 g), (C): 1-fluoro-isocyanatobenzene (0.00084 mol, 0.115 g), the mixture was stirred at 40–50 °C for 6 h, and then maintained stirring overnight. Under reduced pressure, half of the solvent was removed, and the residue was poured into ice. The precipitate was filtered off, and washed with ice-cold EtOH, to yield a product, and recrystallized from 70% EtOH.

*N-(4-bromophenyl)-2-(2-((3-(trifluoromethyl) phenyl) amino) nicotinoyl) hydrazine-1-carboxamide (**3A**)*

Light yellow powder, yield (50%), m.p = (232–234 ^{0}C), R_f = 0.28. ATR-FTIR (ύ, cm^{-1}): 3336, 3213 (NH) str of *sec* amide, 1665 (C = O) str. of amide (amide I band), 1594 (C = N) str, 1564, 1534, 1469 Ar (C = C) str, 1406 (C-F) str, 1332 (C-N) str, 694 (Ar- *p*- Br-substitution).

^{1}HNMR (300MHz, $DMSO_{d6}$, δ = ppm): 10.86 (s, 1H, NH), 10.58 (s,H, 1NH), 9.15 (s, 1H, NH), 8.42–8.21 (m, 3H, Ar-H), 7,88 (d, 1H, Ar-H), 7.52–6.99 (m, 6H, Ar-H).

^{13}CNMR (75MHz, $DMSO_{d6}$, δ = ppm): 158.66 (C = O), 157.14 (ArC = N), 151.38 (C = O), 150.00, 144.47, 141.30, 140.60, 135.99, 129.98, 125.45, 123.31 (CF_3), 118.51, 117.02, 115.44, 115.22, 103.64.

MS (ESI) m/z: Calcd. for $C_{20}H15BrF_3N_5O_2$ $[M+1]^+$ 494.04, found 494.2.

*N-(4-chlorophenyl)-2-(2-((3-(trifluoromethyl) phenyl) amino) nicotinoyl) hydrazine-1-carboxamide (**3B**)*

Dark yellow powder, yield (40%), m.p = (293–295 ^{0}C), R_f = 0.28, ATR-FTIR (ύ, cm^{-1}): 3336,3211 (NH) str. of *sec* amide, 1668 (C = O) str. of amide (amide I band), 1594 (C = N) str, 1531, 1469, 1445 Ar (C = C) str, 1406 (C-F) str1332 (C-N) str, 831 (Ar- p-Cl-substitution).

^{1} HNMR (300MHz, $DMSO_{d6}$, δ = ppm): 10.69 (s, 1H, NH), 10.58 (s,H, NH), 9.15 (s,1H,NH), 8.42–8.18 (m, 3H, Ar-H), 7.88 (d, 1H, Ar-H), 7.55–7.46 (m, 4H, Ar-H), 7.34–7.31 (d, 2H, Ar-H), 6.99 (t, 1H, Ar-H).

^{13}CNMR (75MHz, $DMSO_{d6}$, δ = ppm): 167.67 (C = O), 155.58 (ArC = N), 153.77 (C = O), 150.84, 140.90, 138.47, 137.31, 131.36, 129.79, 128.47, 125.67, 122.82 (CF_3), 120.25, 117.80, 115.07, 114.41, 111.02.

MS (ESI) m/z: Calcd. for $C_{20}H_{15}ClF_3N_5O_2$ $[M-2]^+$ 447.09, found 447.2

*N-(4-fluorophenyl)-2-(2-((3-(trifluoromethyl) phenyl) amino) nicotinoyl) hydrazine-1-carboxamide (**3C**)*

White powder, yield (47%), m.p = (210–213 ^{0}C), R_f = 0.28. ATR-FTIR (ύ, cm^{-1}): 3359,3193 (NH) str. of *sec* amide, 1662 (C = O) str. of amide (amide I band), 1594 (C = N) str, 1567, 1531, 1469Ar (C = C) str, 1409 (C-F) str, 1329 (C-N) str, 1108 (Ar- *p*-F-substitution).

^{1}HNMR (300MHz, $DMSO_{d6}$, δ = ppm): 9.81 (s, 1H, NH), 8.67 (s, 2H, 2NH), 7.48–7.09 (m, 11H, Ar-H).

^{13}CNMR (75MHz, $DMSO_{d6}$, δ = ppm): 152.29 (C = O), 152.26, 142.42, 138.46, 130.49, 124.09 (CF_3), 123.09, 122.98, 119.29, 119.23, 117.16, 117.09, 116.41, 166.11, 115.35.

MS (ESI) m/z: Calcd. fo $C_{20}H_{15}F4N_5O_2$ $[M]^+$ 433.12, found 433.9

General method for synthesis of niflumic hydrazine- carbothioamide derivatives (4A, 4B, 4C, and 4D) (Abbas et al. 2021)

Compound (**2**) (0.25 g, 0.00084 mol) was taken and dissolved in 25 mL of EtOH, then added separately (A): 4-isothiocyanatobenzene (0.00084 mol, 0.11 g), (B): 1-bromo-4-isothiocyanatobenzene (0.00084 mol, 0.18 g), (C): 1-chloro 4-isothiocyanato benzene (0.00084 mol, 0.15 g), (D): 1-isothiocyanato-4-nitrobenzene (0.00084 mol, 0.15 g) the reaction mixture was stirred in water bath at 40–50^{0}C for 6 h , then kept stirring overnight. Under reduced pressure, half of the solvent was removed, and the residue was poured into ice. The precipitate was filtered off, and washed with ice-cold EtOH to produce a product, which recrystallized from 70% EtOH.

*N-phenyl-2-(2-((3-(trifluoromethyl) phenyl) amino) nicotinoyl) hydrazine-1-carbothioamide (**4A**)*

Yellow powder, yield (88%), m.p = (195–198 ^{0}C), R_f = 0.55, ATR-FTIR (ύ, cm^{-1}): 3243 (NH) str of *sec* amide, 3163 (NH) str of thioamide, 1668 (C = O) str. of amide (amide I band), 1614 (C = N) str, 1591 (NH) bend , 1525, 1492, 1463, Ar (C = C) str, 1394 (C-F) str, 1329 (C-N) str , 1251 (C = S) str.

^{1}HNMR (300MHz, $DMSO_{d6}$, δ = ppm): 10.86 (s, 2H, 2NH), 9.89 (s, 1H, NH), 9.75 (s, 1H, NH), 8.44–8.26 (m.3H, Ar-H), 7.86 (t, 1H, Ar-H), 7.54–7.33 (m, 6H, Ar-H), 7.18 (s, 1H, Ar-H), 7.00 (t, 1H, Ar-H).

^{13}CNMR (75MHz, $DMSO_{d6}$, δ = ppm): 181.12 (C = S), 162.30 (C = O), 154.02 (Ar = CN), 151.06, 140.82, 139.03, 137.88, 129.82, 129.28, 128.00, 126.04, 125.06, 122.98 (CF_3), 117.89, 115.13, 114.26.

MS (ESI) m/z: Calcd. for $C_{20}H_{16}F_3N_5OS$ $[M]^+$ 431.10, found 431.9.

*N-(4-bromophenyl)-2-(2-((3-(trifluoromethyl) phenyl) amino) nicotinoyl) hydrazine-1-carbothioamide (**4B**)*

Yellow powder, yield (85%), m.p = (175–178 ^{0}C), R_f = 0.58, ATR-FTIR (ύ, cm^{-1}): 3309 (NH) str of *sec* amide, 3151 (NH) str of thioamide, 1644 (C = O)str. of amide (amide

I band), 1603 (C = N) str, 1549, 1531, 1492Ar (C = C) str, 1403 (C-F) str, 1326 (C-N) str, 1251 (C = S) str , 766 (Ar-*p*- Br-substitution).

^{1}HNMR (300MHz, $DMSO_{d6}$, δ = ppm): 10.87 (s, 1H, NH), 9.87 (s, 1H, NH), 8.45–8.26 (m, 3H, Ar-H), 7.85 (d, 1H, Ar-H), 7.54–7.30 (m, 6H, Ar-H), 7.01 (t, 1H, Ar-H).

^{13}CNMR (75MHz, $DMSO_{d6}$, δ = ppm): 181.57, 168.03, 162.79, 151.73, 141.27, 138.97, 138.42, 131.33, 130.33, 128.49, 126.10, 125.61, 123.54, 118.43, 115.66, 114.74, 110.39.

MS (ESI) calcd. for $C_{20}H_{15}BrF_3N_5OS$ $[M+1]^+$ 510.01, found 510.50

*N-(4-chlorophenyl)-2-(2-((3-(trifluoromethyl) phenyl) amino) nicotinoyl) hydrazine-1-carbothioamide (**4C**)*

Light yellow powder, yield (80%), m.p = (169–172 ^{0}C), R_f = 0.58.ATR-FTIR (ύ, cm^{-1}): 3312 (NH) str of *sec* amide, 3160 (NH) str. of thioamide, 1647 (C = O) str. of amide (amide I band), 1603 (C = N) str, 1549, 1495, 1445Ar (C = C) str, 1406 (C-F) str, 1329 (C-N) str, 1248 (C = S) str, 825 (Ar- *p*- Cl-substitution).

^{1}HNMR (300MHz, $DMSO_{d6}$, δ = ppm): 10.87 (s, 1H, NH), 9.86 (s, 2H, NH), 8.44 (d, 1H, Ar-H), 8.33–8.26 (m, 2H, Ar H), 7.83 (d, 1H, Ar-H), 7.54–7.33 (m, 6H, Ar-H), 7.02 (t, 1H, Ar-H).

^{13}CNMR (75MHz, $DMSO_{d6}$, δ = ppm): 169.94, 168.01, 162.78, 154.60, 151.75, 141.27, 138.54, 130.33, 129.84, 128.68, 128.41, 128.14, 126.10, 123.54, 118.42, 115.65, 114.74, 110.33.

MS (ESI) calcd. for $C_{20}H_{15}ClF_3N_5OS$ $[M+1]^+$ 466.06, found 466.00 .

*N-(4-nitrophenyl)-2-(2-((3-(trifluoromethyl) phenyl) amino) nicotinoyl) hydrazine-1-carbothioamide (**4D**)*

Yellow powder, yield (74%), m.p = (171–173 ^{0}C), R_f = 0.56. ATR-FTIR (ύ, cm^{-1}): 3309 (NH) str of *sec* amide, 3148 (NH) str. of thioamide, 1647 (C = O) str. of amide (amide I band), 1603 (C = N) str, 1561, 1531, 1445Ar (C = C) str, 1510, 1335 *asym/sym*. str. of NO_2 group, respectively, 1412 (C-F) str , 1335 (C-N) str, 1251 (C = S) str.

^{1}HNMR (300MHz, $DMSO_{d6}$, δ = ppm): 10.97 (s, 1H, NH), 10.85 (s, 1H, NH), 10.21 (s, 1H, NH), 8.46 (s, 1H, Ar-H), 8.33–8.21 (m, 4H, Ar-H), 7.91–7.83 (m, 3H, Ar-H), 7.54 (d, 1H, Ar-H), 7.32 (d, 1H, Ar-H), 7.02 (t, 1H-Ar-H).

^{13}CNMR (75MHz, $DMSO_{d6}$, δ = ppm): 181.10 (C = S), 167.85 (C = O), 154.46 (ArC = N), 151.68, 145.82, 143.82 (C-NO_2), 141.01, 138.16, 130.09, 125.87, 125.26, 123.88 (CF_3), 123.37, 118.24, 115.52, 114.58, 110.01.

MS (ESI) Calcd. for $C_{20}H_{15}F_3N_6O_3S$ $[M+1]^+$ 477.09, found 477.30.

General method for synthesis of niflumic1,2,4-triazole-3-thione derivatives (5A,5B, and 5C) (Abdul- Jabbar et al. 2005)

The hydrazine carbothioamide compounds (**4B, 4C**, and **4D**) (0.001 mol) were separately added to 2N NaOH (6.6 mL), stirred at RT for (15 min), when a clear yellow solution appeared, then it was refluxed for 3 h. Before acidifying with 2N HCl to pH = 3, the reaction mixture was cooled to room temperature. The resulting solid was filtered, and recrystallized from 70% EtOH, to afford the corresponding final compounds **(5A,5B and 5C).**

*4-(4-bromophenyl)-5-(2-((3-(trifluoromethyl) phenyl) amino) pyridin-3-yl)-2,4-dihydro-3H-1,2,4-triazole-3-thione (**5A**)*

Yellow powder, yield (65%), m.p = (200–203 ^{0}C), R_f= 0.82. ATR-FTIR (ύ, cm^{-1}): 3342 (NH) str. of *sec* amine, 3097 Ar (CH) str, 2758 (SH) str. 1677 (C = N) str, 1594, 1540, 1486Ar (C = C) str, 1329 (C-N) str, 1281 (C = S) str, 763 (Ar-*p*-Br-substitution).

^{1}HNMR (300MHz, $DMSO_{d6}$, δ = ppm): 11.07 (s, 1H, NH), 10.24 (s, 1H, NH), 8.39 (d, 1H, Ar-H) 8.09–7.92 (dd, 2H, Ar-H), 7.94(d,1H,Ar-H), 7.61–7.09 (dd, 8H, Ar-H).

^{13}CNMR (75MHz,$DMSO_{d6}$, δ = ppm): 159.12, 156.55, 151.32, 149.71 (C = N), 140.67, 137.70, 135.70, 131.88, 129.96, 129.78, 123.29 (CF_3), 119.24, 118.44, 115.39, 115.19, 113.72, 103.85.

MS (ESI) Calcd. for $C_{20}H_{13}BrF_3N_5S[M+1]^+$ 492.00, found 492.10.

*4-(4-chlorophenyl)-5-(2-((3-(trifluoromethyl) phenyl) amino) pyridin-3-yl)-2,4-dihydro-3H-1,2,4-triazole-3-thione (**5B**)*

White powder, yield (60%), m.p = (215–218 ^{0}C), R_f= 0.73. ATR-FTIR (ύ, cm^{-1}): 3318 (NH) str. of *sec*, amine, 3100 Ar (CH) str, 1650 (C = N) str, 1588, 1498, 1442Ar (C = C) str, 1385 (C-F) str, 1329 (C-N) str, 1251 (C = S) str, 763 (Ar-*p*-Cl-substitution).

^{1}HNMR (300MHz, $DMSO_{d6}$, δ = ppm): 14.26 (s, 1H, NH), 10.25 (s, 1H, NH), 8.76 (s, 1H, Ar-H), 8.26 (t, 1H, Ar-H), 7.73–7.23 (m, 8H, Ar-H), 6.92 (s, 1H, Ar-H).

^{13}CNMR (75MHz, $DMSO_{d6}$,δ = ppm): 167.93 (C = S), 152.33 (ArC = N), 149.81, 147.94, 141.19, 141.02, 133.53 (C-Cl), 132.70, 129.47, 129.20, 128.62, 122.56 (CF_3), 117.37, 115.29, 114.91, 112.16, 108.38.

MS (ESI) Calcd. for$C_{20}H_{13}Cl$ F_3N_2S $[M]^+$ 447.05, found 447.90.

*4-(4-nitrophenyl)-5-(2-((3-(trifluoromethyl) phenyl) amino) pyridin-3-yl)-2,4-dihydro-3H-1,2,4-triazole-3-thione (**5C**)*

Dark yellow powder, yield (60%), m.p = (240–243 ^{0}C), R_f = 0.79, ATR-FTIR (ύ, cm^{-1}): 3431, 3330 (NH) str. of each *sec*, amine & cyclic thioamide, 2856 (SH) str, 1674 (C = N) str, 1632, 1591, 1457Ar (C = C) str, 1528, 1329 *asym/sym*. str. of NO_2, respectively, 1415 (C-F) str, 1329 (C-N) str, 1248 (C = S) str.

^{1}H-NMR (300MHz, $DMSO_{d6}$,δ = ppm): 10.21 (s, 1H, NH), 8.47–8.30 (m, 4H, Ar-H), 8.13 (d, 1H, Ar-H) 7.95–7.85 (m, 3H, Ar-H), 7.38 (m, 1H, Ar-H), (dd, 7.12, 1H, Ar-H).

^{13}CNMR (75MHz, $DMSO_{d6}$, δ = ppm): 158.66 (ArC = N), 157.14, 151.38, 150.00, 144.47 (C-NO_2), 141.30, 140.60, 135.99, 129.98, 125.45, 123.31, 117.02, 115.44, 115.39, 115.22, 103.64

MS (ESI) Calcd. for $C_{20}H_{13}F_3N_6O_2S$ $[M+1]^+$ 459.08, found 459.30.

Synthesis of 4-(4-chloro-phenyl)-5-(2-((3-(trifluoromethyl) phenyl) amino) pyridin-3-yl)-2,4-dihydro-3H-1,2,4-triazol-3-one (6) (Abdul- Jabbar et al. 2005)

Hydrazine carboamide compound (**3B**) (0.001 mol**, 0.25 g**) was added to 2N NaOH (6.6 mL), stirred at RT for 15 min, a clear yellow solution appeared which was refluxed for 3 h. The reaction mixture was cooled at RT, until being acidified with 2N HCl, to obtain a pH of 3. The resulting solid was filtered and recrystallized from 70% EtOH to produce the corresponding final compound (**6**).

Yellow powder, yield (47%), m.p = (230–233 ^{0}C), R_f = 0.77. ATR-FTIR (ύ,cm^{-1}): 3333, (NH) str. of *sec.* amine, 3208 str of NH cyclic *amide*, 1665 (C = O) str, 1591 (C = N) str, 1564, 1531, 1445Ar (C = C) str, 1406 (C-F) str, 1329 (C-N) str, 766 (Ar-*p*-Cl-substitution).

^{1}HNMR (300MHz, DMSO$_{d6}$, δ = ppm): 10.69–10.58 (s, 2H, 2NH), 9.15 (s, 1H, OH (enolic form), 8.42–8.18 (m, 4H, Ar-H), 7.88 (d, 1H, Ar-H), 7.55–7.00 (m, 6H, Ar-H).

^{13}CNMR (75MHz, DMSO$_{d6}$, δ = ppm): 167.67, 155.58, 153.75, 150.84, 140.90, 138.45, 137.31, 131.42

(C-Cl), 129.80, 128.47, 125.69, 122.81 (CF_3), 120.33, 120.26, 117.76, 115.06, 114.42.

MS (ESI) Calcd. for $C_{20}H_{13}ClF_3N_5O[M+NH_4]^+$ 449.80, found 449.90.

Synthesis of novel niflumic acid (NF) derivatives is depicted in scheme 1.

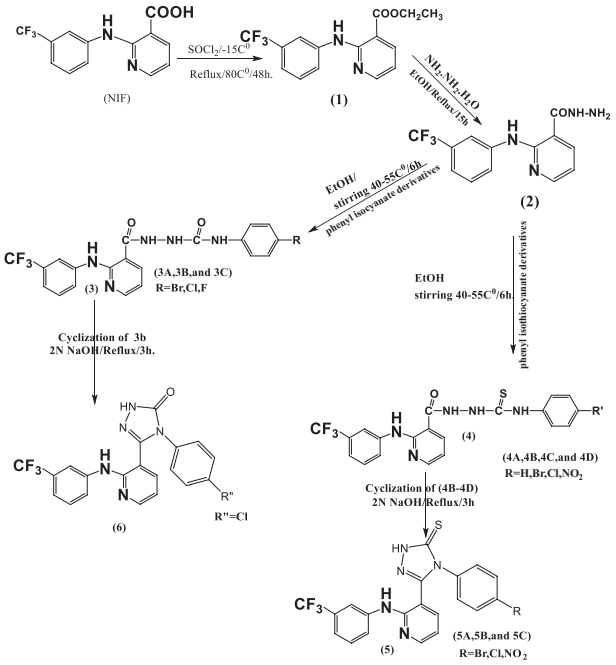

Scheme 1. Chemical synthesis of niflumic acid (NF) derivatives.

Molecular docking study

For the molecular docking process, the CDOCKER protocol was used. The receptor was kept rigid during the method, while the ligands were made flexible. Each molecule was allowed to create ten different interaction poses with the protein. When the best-fitting poses were identified, docking scores (-CDOCKER interaction energy) were noted. The protein data bank (https://www.rcsb.org) was used to identify molecular targets for the newly synthesized compounds **(3A–6),** compare them to other ligands, and determine the pharmacophoric functionality that may enable binding to the critical amino acid(s), at the target site. The hit compounds are assessed in practice against many active sites, and the findings are then used to select the proper protein for molecular docking.

Following the selection of a specific protein, some procedures were performed that provide an understanding of the molecular binding modes of the test compounds inside of the pockets of the proteins (VEGFR tyrosine kinase, and EGFR tyrosine kinase), by using MOE 19.0901 Software. The co-crystallized ligand was used to produce the binding sites within the crystal protein (PDB codes: 1YWN-4HJO) (https://www.rcsb.org). Water molecules were initially removed from the complex. The crystallographic disorders, and unfilled valence atoms were then corrected using protein report, utility, and clean protein options. Protein energy was minimized by applying MMFF94 force fields to it. Trying to apply a fixed atom constraint contributed to making the structure of the protein rigid. The essential amino acids of the protein are outlined and ready for docking. The 2D structures of the compounds tested were sketched in Chem-Bio Draw Ultra17.0, and saved in MDL-SD file format using MOE 19.0901 software. The saved file was opened, 3D structures protonated, and energy was kept to a minimum by using a .05 RMSD kcal/mol MMFF94 force field. The minimized structures were then ready for docking with the prepared ligand protocol.

Biological study

Cell culture

Three human cell lines were used in the current study, the lung fibroblast normal cell line WI-38, and two cancer cell lines: A549 lung cancer cell line, and Hep G2 hepatocyte carcinoma cell line. WI-38 and Hep G2 cell lines were cultured in Eagle's minimum essential medium (LONZA, Switzerland) supplemented with 10% fetal bovine serum (FBS; Gibco, USA), while A549 lung cancer cell line was cultured in Ham's F-12K medium (Thermo Scientific, USA) supplemented with 10% FBS. Cells were passaged using trypsin-EDTA (Millipore-Merck, USA), and maintained at 37 °C in 5% CO_2 and 95% air.

Analysis of cytotoxicity by the in vitro MTT assay

The MTT assay was used to evaluate the cytotoxicity of the newly synthesized NF derivatives against the different cell lines (Mosmann 1983). Viable metabolically active cells were able to reduce the yellow tetrazolium salt (3-(4,5-dimethylthiazol-2-yl)-2,5-diphenyltetrazolium bromide or MTT salt) to purple formazan crystals, which were then dissolved using a solubilization solution (1:1 DMSO and

isopropanol mixture). The resulting-colored solution was quantified by measuring absorbance at 590 nm using Multiskan EX (Thermo Scientific, USA) Microplate Reader. The experiment was performed three times in triplicates.

Cell cycle analysis by flow cytometry

Flow cytometry was used to estimate the percentage of a cell population in the different phases of cell cycle (sub-G1, G1, S, and G2/M). Control and compound **4C**-treated Hep G2 cancer cells (IC_{50}, 48 h) were fixed, and stained with propidium iodide (PI). The fluorescence of the PI-DNA complex was detected using Epics XL-MCL Flow Cytometer (Beckman Coulter), and the Flowing software (version 2.5.1, Turku Centre for Biotechnology, Turku, Finland) was used to analyze the cell distribution at different stages of the cell cycle (Nunez 2001),(Pozarowski and Darzynkiewicz 2014).

Detection of viable, apoptotic, and necrotic cells by flow cytometry

The Elabscience (USA) Annexin V-FITC / PI Cell Apoptosis Detection kit was used to identify viable, apoptotic, and necrotic cells. Control and compound **4C**-treated Hep G2 cells (IC_{50} concentration, 48 h) were fixed, and stained with Annexin V-FITC, and propidium iodide (PI). Viable, apoptotic (early or late), or necrotic cells were distinguished by flow cytometry.

Analysis of apoptosis markers gene expression by quantitative reverse transcription-polymerase chain reaction (qRT-PCR)

Total RNA from control and compound **4C**-treated (IC_{50}, 48 h) cells was extracted following manufacturer's instructions (RNeasy mini kit, Qiagen, Germany). RNA was reverse transcribed to cDNA using the Revert Aid First Strand cDNA Synthesis kit (Thermo Scientific, USA), and assayed for p53, BAX, Bcl-2, and caspase-3 gene expression (mRNA level) by quantitative RT-PCR (qRT-PCR). GAPDH was used as the housekeeping (normalization) gene. 2 µL cDNA were mixed with 1 µL of forward primer, 1 µL reverse primer **(Table 1),** 10 µl master mixture, and 6 µL nuclease-free water. Experiments were performed in triplicate.

Vascular endothelial growth factor receptor 2 (VEGFR2) and epidermal growth factor receptor (EGFR) kinase inhibitory assay

The VEGFR2 Kinase Assay Kit and the EGFR kinase Assay Kit (BPS Bioscience, USA) were used to assess the inhibitory activities of compound **4C** and compound **5B**, respectively, using the Kinase-Glo MAX (Promega, USA), as a detection reagent. Eight different concentrations of each compound (1000, 300, 100, 30, 10, 3, 1, and 0.3 nM) were prepared, and tested following the manufacturer's instructions. The concentration-percent remaining kinase activity (% inhibition) curve was used to calculate the concentration that caused 50% kinase activity inhibition (the effective concentration that inhibits 50% of kinase activity; EC_{50}). The experiment was performed three times in triplicate.

Statistical analysis

Data presented in the current study are expressed as mean ± SEM of three independent experiments. GraphPad software (GraphPad Prism version 8.0, San Diego, CA, USA) was used to perform statistical analysis. Student's t-test was used to determine significance between means, p value < 0.05 was considered significant.

Results and discussion

Docking study

All of these procedures are used to anticipate the proposed binding mode, affinity, and preferred orientation for each docking pose, and the binding scored energy (ΔG) of the compounds examined against VEGFR tyrosine Kinase, and EGFR tyrosine Kinase (Seidel et al. 2020) (Table 2). The measured interaction energies for the examined samples were all consistent with the observed results, implying that compound **3A** may have potent inhibitory activity against VEGFR tyrosine kinase, while compound **5C** may act against EGFR tyrosine kinase.

The crystal ligand's (analogue of sorafenib) binding mode exhibited an energy of -7.10 kcal/ mol against VEGFR tyrosine kinase. In which the 4-amino furo [2,3-d] pyrimidin-5-yl moiety formed eight *pi-pi*, and *pi*-alkyl interactions with Val846, Leu838, Leu1033, Phe916, Cys917, and Ala864. Additionally, binding with Glu183 and Cys917 by two H-bonds with a distance of 1.83 and 2.05 °A. The 4-chloro -3-(trifluoromethyl) phenyl) urea moiety formed seven *pi*-alkyl interactions with Val914, Cys1043, Val897, Ala864, Leu1017, Ile890, Leu887, and five H- bonds with Asp1044, Glu883, and Ile1042 (1.83, 1.87, 3.54, 1.95 and 3.47 °A). On the other hand, the 4-methoxy phenyl moiety formed a *pi*-alkyl interaction with Val846. (Fig. 1).

The binding mode of the crystal ligand (erlotinib) displayed a binding's energy of -7.95 kcal/ mol against EGFR tyrosine kinase. The quinazolin-4-amine ring established three *pi*-alkyl interactions with Leu694, Ala719, and Leu820. Furthermore, the amino group in the qui-

Table 1. Sequence of qRT-PCR primers, forward (F) and reverse (R), used in the current study.

Gene	Primer sequence	Reference
P53	F: 5'- GCCCAACAACACCAGCTCCT -3' R: 5'- CCTGGGCATCCTTGAGTTCC -3'	(Zhang et al. 2019)
BAX	F: 5'- CCCGAGAGGTCTTTTTCCGAG -3' R: 5'- CCAGCCCATGATGGTTCTGAT -3'	(Jiang et al. 2020)
Bcl-2	F: 5'- TTGTGGCCTTCTTTGAGTTCGGTG -3' R: 5'- GGTGCCGGTTCAGGTACTCAGTCA -3'	(Khodapasand et al. 2015)
Caspase-3	F: 5'- ACATGGAAGCGAATCAATGGACTC -3' R: 5'- AAGGACTCAAATTCTGTTGCCACC -3'	(Peluffo et al. 2005)
GAPDH	F: 5'- GACCCCTTCAT GACCTCAAC -3' R: 5'- CTTCTCCATGGTGGT GAAGA -3'	

Table 2. Binding score energy (ΔG; kcal/mol) of the tested compounds against VEGFR and EGFR tyrosine kinase target site PDB ID: 1YWN and 4HJO.

Ligand	RMSD value (Å)	Docking score (kcal/mol)	Interactions	
			H.B	*pi*-interactions
Crystal ligand (1YWN)	1.36	-7.10	5	15
Compound 3A	1.67	-8.76	2	16
Compound 3B	1.87	-7.87	-	13
Compound 3C	1.50	-8.11	5	9
Compound 4A	1.41	-7.33	5	8
Compound 4B	1.64	-8.58	4	6
Compound 4C	1.09	-8.18	4	10
Compound 4D	1.22	-8.62	4	14
Crystal ligand 4HJO (Erlotinib)	1.39	-7.95	1	5
Compound 5A	1.30	-7.74	4	10
Compound 5B	1.03	-7.78	4	9
Compound 5C	1.55	-9.11	10	11
Compound 6	1.34	-8.17	4	9

nazoline ring interacted with Met769 by one H-bond with a distance of 2.10 °A. While the 3-ethynylphenyl moiety formed two *pi*-alkyl interactions with Val702, and Leu820. (Fig. 2).

The candidate compound **3A**'s binding mode exhibited an energy binding of -8.76 kcal/mol against VEGFR tyrosine kinase. The 3-(trifluoromethyl) phenyl) amino) nicotinoyl moiety, had thirteen *pi*-alkyl and *pi*-*pi* interactions with Ala864, Cys917, Phe916, Leu1033, Leu838, Val914, Lys866, Phe1045, Leu1047 and Val846, and interacted with Cys917 *via* two H- bonds at a distance of 2.18 and 3.18 °A, while the 4-bromophenyl hydrazine-1-carboxamide moiety produced three *pi*-alkyl interactions with Cys1022, Leu1017, and Ile890. In addition, there are two ionic interactions with Asp1044, and Glu883. (Fig. 3).

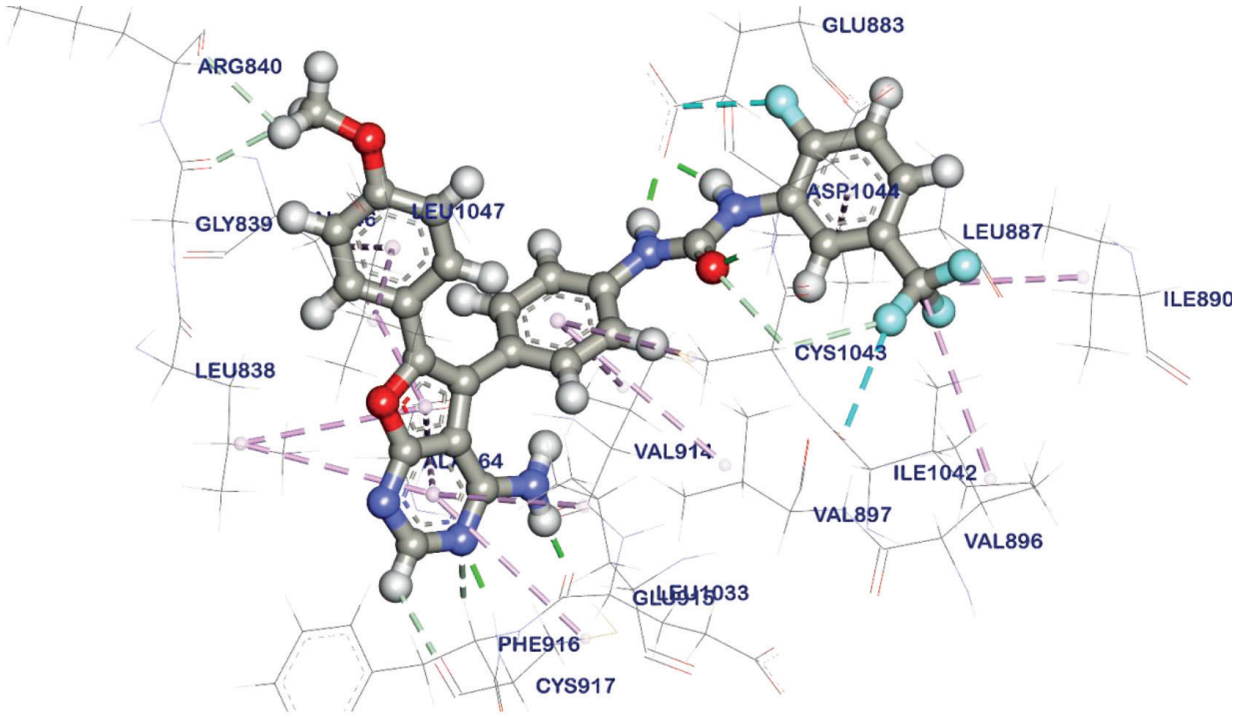

Figure 1. The Crystal ligand (1YWN) docked in VEGFR tyrosine kinase, hydrogen bonds (green lines) and the pi interactions (purple lines) with mapping surface representing the crystal ligand occupying the active pocket of VEGFR tyrosine kinase.

Compound **5C** showed an energy binding of -9.11 kcal/mol against EGFR tyrosine kinase. The 3-(trifluoromethyl) phenyl) amino) pyridin-3-yl moiety formed five *pi*-sulfur and *pi*-alkyl interactions with Val702, Lys721, Leu764, Met742, and Ala719. Moreover, it interacted with Phe832, Cys751, and Arg752 by seven H- bonds (2.75, 2.93, 3.65, 4.91, 3.45, 3.03, and 3.25 °A). The 4-nitrophenyl-1,2,4-triazole-3-thione moiety produced six *pi*-alkyl interactions with Leu694, Leu820, Ala719, and Val702, and three H- bonds with Met769, Arg817, and Asp831 (2.09, 3.49, and 2.56 °A) (Fig. 4).

Molecular Similarity

A molecular similarity study was performed for eleven ligands that showed anticancer activities against VEGFR-2 tyrosine kinase, and EGFR tyrosine crystal ligands using the Discovery Studio software. The used molecular properties included the number of rotatable bonds, number of cyclic rings, number of aromatic rings, number of hydrogen bond donors (HBD), number of hydrogen bond acceptors (HBA), partition coefficient (Log p), molecular weight (M.Wt.), and molecular fractional polar surface area (MFPSA) (Fig. 5) and (Table 3).

ADMET studies

The findings of the ADMET studies (absorption, distribution, metabolism, excretion, and toxicology), were measured using Biovia Discovery Studio 2019. They revealed that blood penetration levels of the brain-blood barrier (BBB) of all ligands ranged from medium to low, indicating a lower possibility for CNS side effects. Additi-

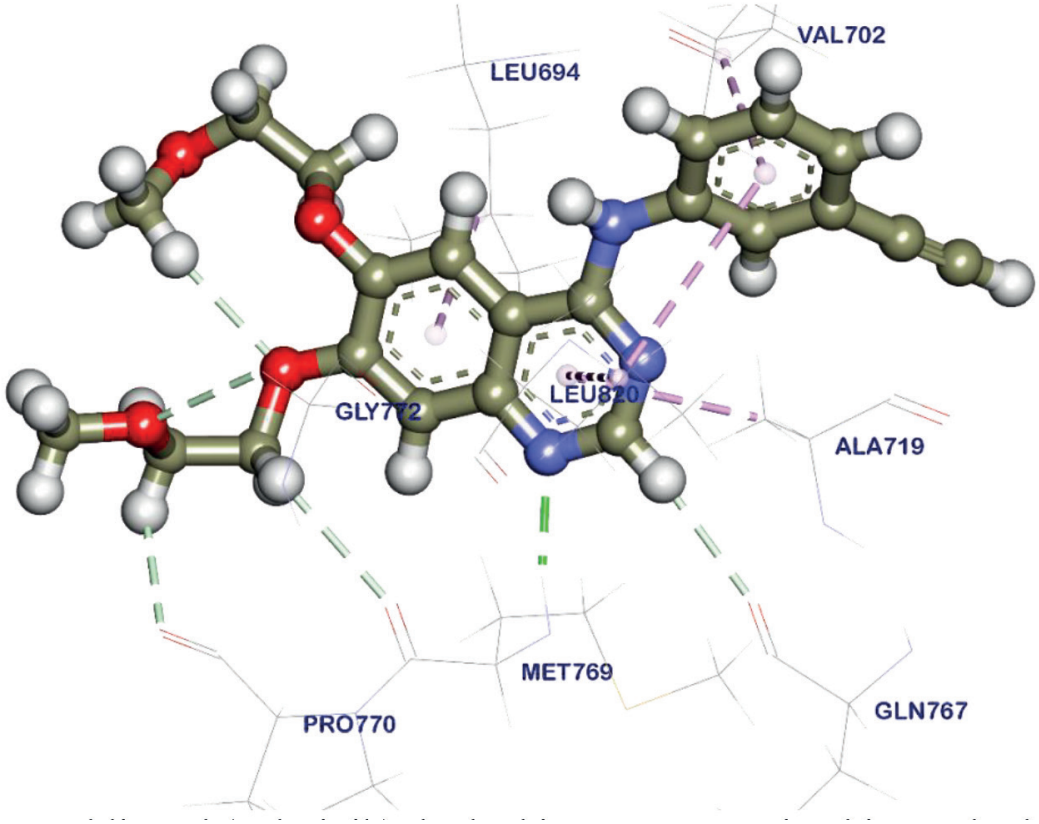

Figure 2. The Crystal ligand (Erlotinib) docked in EGFR tyrosine kinase, hydrogen bonds (green lines) while the pi interactions are shown in purple lines, with mapping surface showing the crystal ligand dominating the active site of EGFR tyrosine kinase.

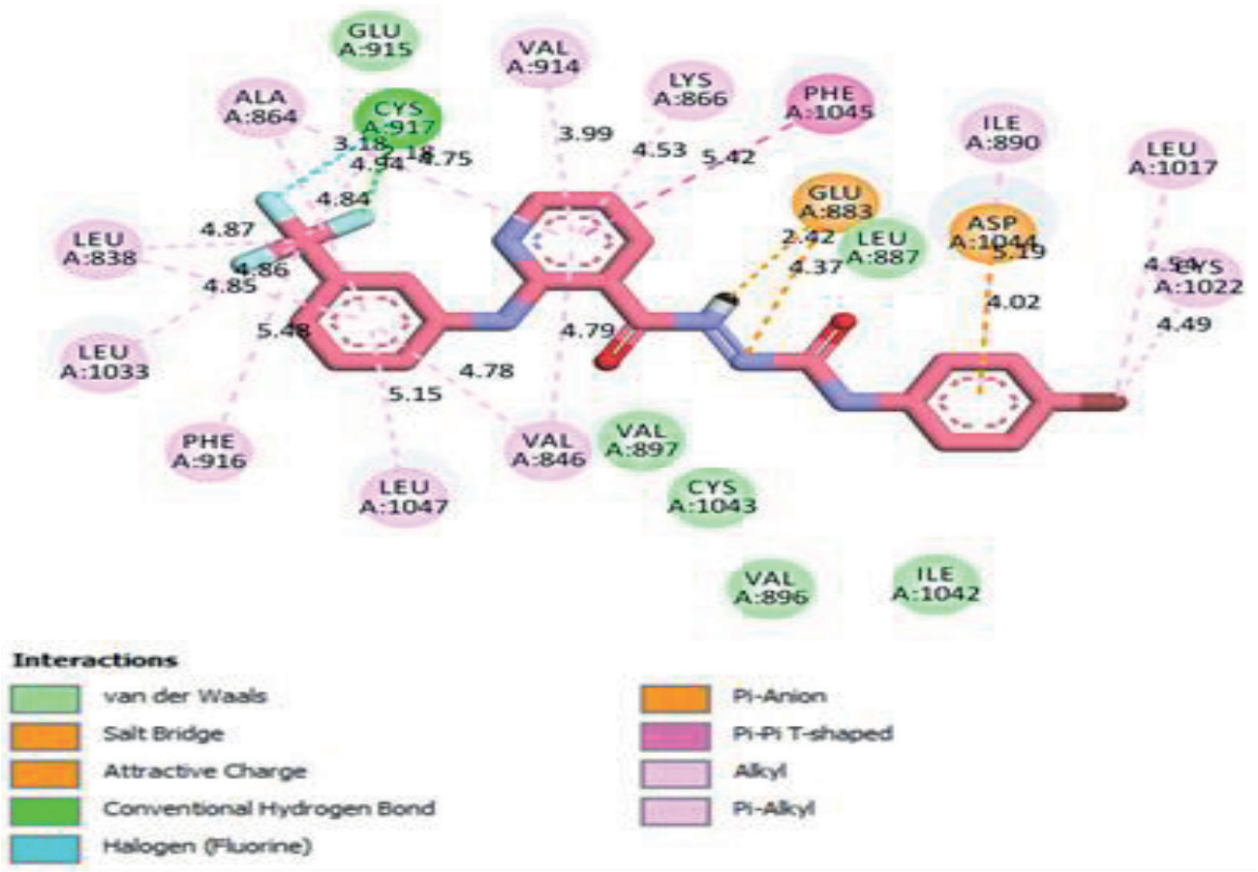

Figure 3. Compound **3A** docked in VEGFR tyrosine kinase, hydrogen bonds (green lines), the pi interactions are depicted in purple lines, and the mapping surface proves compound **3A** directly binds to the active pocket of VEGFR tyrosine kinase.

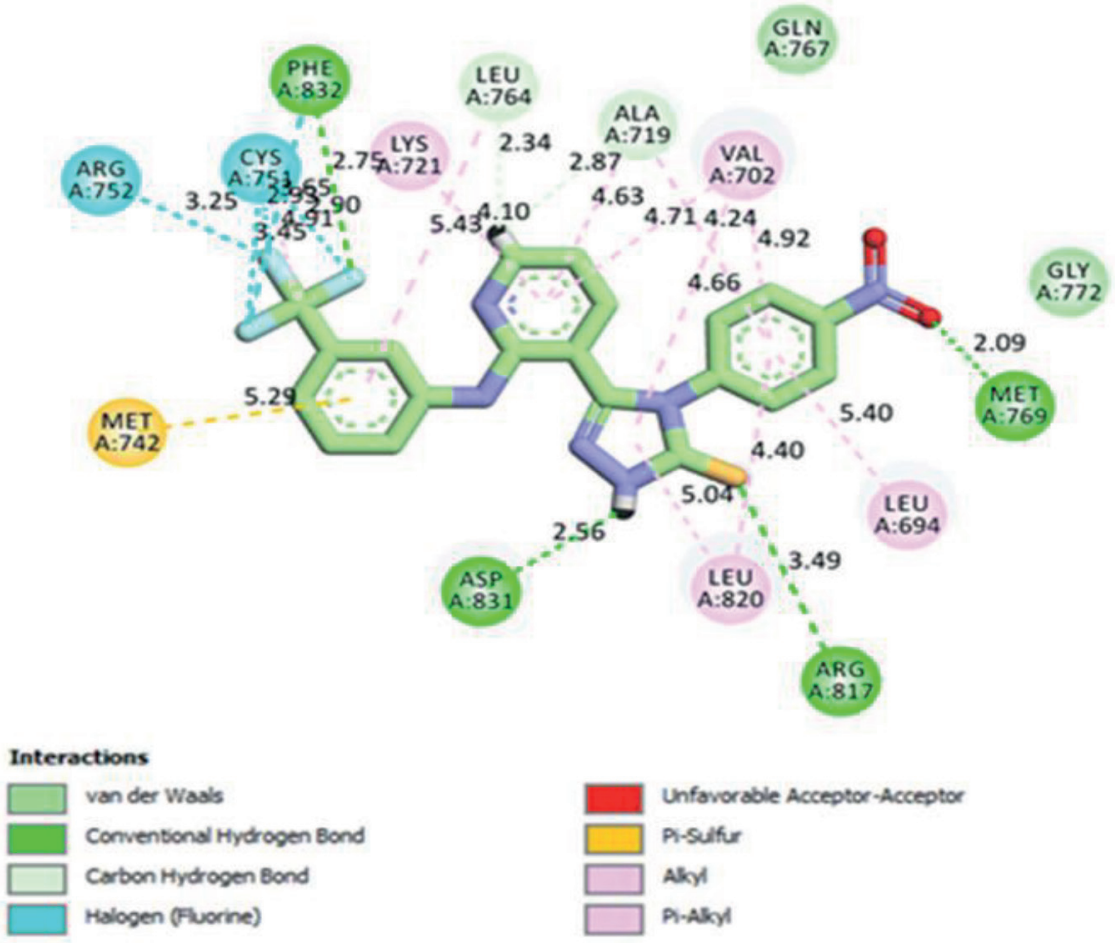

Figure 4. Compound **5C** docked in EGFR tyrosine kinase, hydrogen bonds are represented in green lines, while the pi interactions are represented in purple lines.

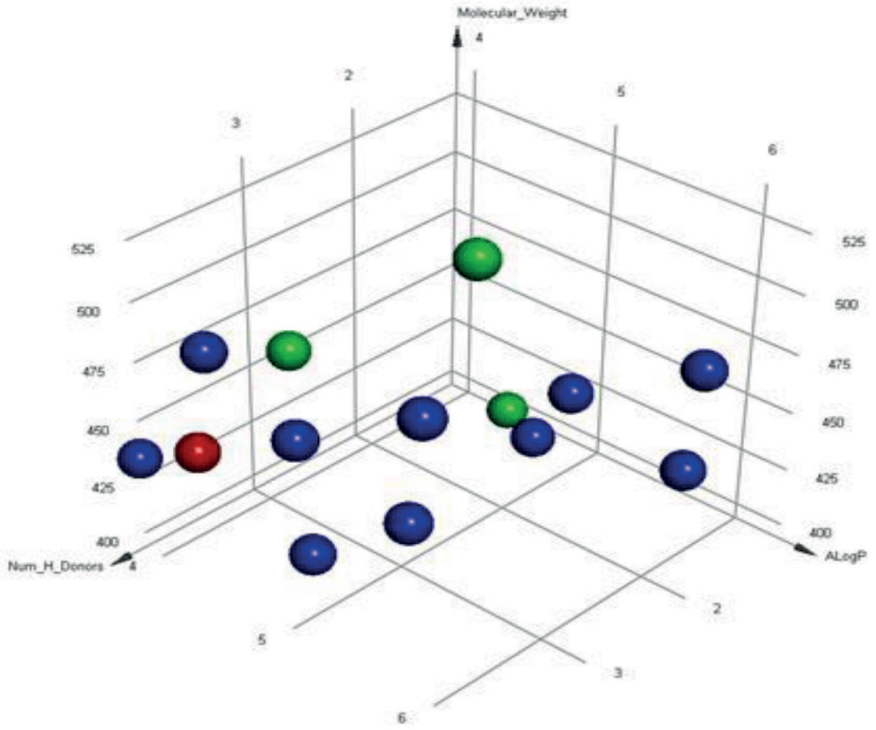

Figure 5. The similarity analysis between the tested molecules and VEGFR-2 tyrosine kinase and EGFR tyrosine kinase crystal ligands. Green ball = crystal ligands (reference), red ball = similar ligand (**3A**), blue balls = dissimilar ligands.

Table 3. The results of the molecular properties including partition coefficient (Log p), molecular weight (M.Wt.), number of hydrogen bond donors (HBD), number of hydrogen bond acceptors (HBA), the number of rotatable bonds, number of cyclic rings, number of aromatic rings, molecular fractional polar surface area (MFPSA), and minimum distance.

Comp.	Log p	M. Wt	HBA	HBD	Rotatable bonds	Rings	Aromatic rings	MFPSA	Minimum Distance
3A	4.409	494.265	4	4	6	3	3	0.229	0.479711
3B	4.325	449.814	4	4	6	3	3	0.231	0.405977
3C	3.866	433.359	4	4	6	3	3	0.237	0.519793
4A	5.155	431.434	4	4	8	3	3	0.273	0.925923
4B	5.903	510.33	4	4	8	3	3	0.257	1.13235
4C	5.819	465.879	4	4	8	3	3	0.259	1.01524
4D	5.049	476.432	6	4	9	3	3	0.353	1.56193
5A	6.307	492.315	4	2	5	4	3	0.209	1.23722
5B	6.223	447.864	4	2	5	4	3	0.211	1.18748
5C	5.453	458.416	6	2	6	4	3	0.313	1.37821
6	5.201	431.798	4	2	5	4	3	0.18	0.938916
Crystal ligand (1YWN)	5.499	537.465	5	3	6	5	5	0.228	–
Erlotinib	4.309	393.436	7	1	10	3	3	0.177	–
Sorafenib	4.175	464.825	4	3	6	3	3	0.212	–

onally, all ligands had low solubility levels. Furthermore, most the tested ligands showed good absorption levels and appeared to be non-inhibitors for cytochrome P_{450}. Concerning hepatotoxicity, all ligands were predicted to be non-hepatotoxic, compared with sorafenib and erlotinib, which showed some levels of *in silico* hepatotoxicity. Finally, some ligands were predicted to bind plasma protein (PPB) by more than 90%. These findings indicate that all ligands have good pharmacokinetic properties, and accordingly, they were preferred for further investigations (Table 4), and (Fig. 6).

Density Functional Theory (DFT)

The most promising ligands (**3A, 4D**, and **5C**) were chosen for DFT studies to investigate their electronic profiles. DFT goal is the quantitative understanding of material properties from the fundamental law of quantum mechanics. The Discovery studio software was utilized in this test. Crystal ligand (1 ywn), and Erlotinib were utilized, as reference molecules. The calculated DFT parameters include the total energy of the molecules, binding energy, energy of the highest occupied molecular

Table 4. Predicted ADMET results for the synthesized (NF) derivatives.

Compound	BBB level[a]	Solubility level[b]	Absorption level[c]	Hepatotoxicity	CYP2D6 prediction	PPB prediction[e]
3a	4	1	0	*False*	*False*	*True*
3b	4	1	0	*False*	*False*	*True*
3c	4	1	0	*False*	*False*	*True*
4a	2	1	0	*False*	*False*	*True*
4b	4	1	1	*False*	*False*	*True*
4c	4	1	1	*False*	*False*	*True*
4d	4	1	2	*False*	*False*	*True*
Sorafenib	4	1	0	*True*	*False*	*True*
Crystal ligand (1YWN)	4	1	1	*False*	*False*	*True*
5a	4	0	2	*False*	*False*	*True*
5b	4	0	2	*False*	*True*	*True*
5c	4	0	2	*False*	*False*	*True*
6	1	1	0	*False*	*True*	*True*
Erlotinib	1	2	0	*True*	*False*	*True*

[a] BBB (blood brain barrier level): 0 = very high, 1 = high, 2 = medium, 3 = low, 4 = very low.
[b] Solubility level: 1 = very low, 2 = low, 3 = good, 4 = optimal.
[c] Absorption level: 0 = good, 1 = moderate, 2 = poor, 3 = very poor.
[d] CYP2D6, cytochrome P2D6: True = inhibitor, False = non inhibitor. The classification of whether a compound is a CYP2D6 inhibitor using the cutoff Bayesian score of 0.161.
[e] PBB, plasma protein binding: False means less than 90%, True means more than 90%. The classification of whether a compound is highly bound (≥ 90% bound) to plasma proteins using the cutoff Bayesian score of -2.209.

orbital (HOMO), the energy of the lowest unoccupied molecular orbital (LUMO), and the magnitude of the dipole moment. The HOMO is coupled with an electron donor ability, while LUMO is linked to the acceptance of electrons. These orbitals describe the way the ligand will interact with other species. The gap energy helps to balance the chemical reactivity with the kinetic stability of a drug. Furthermore, the total dipole moment describes the ability of interaction of a chemical candidate with the surrounding environment. The results of DFT studies are summarized in (Table 5) and (Fig. 7).

Molecular orbital analysis

Compounds **3A, 4C, 4D,** and VEGFR tyrosine kinase crystal ligand (1YWN), showed total energy values

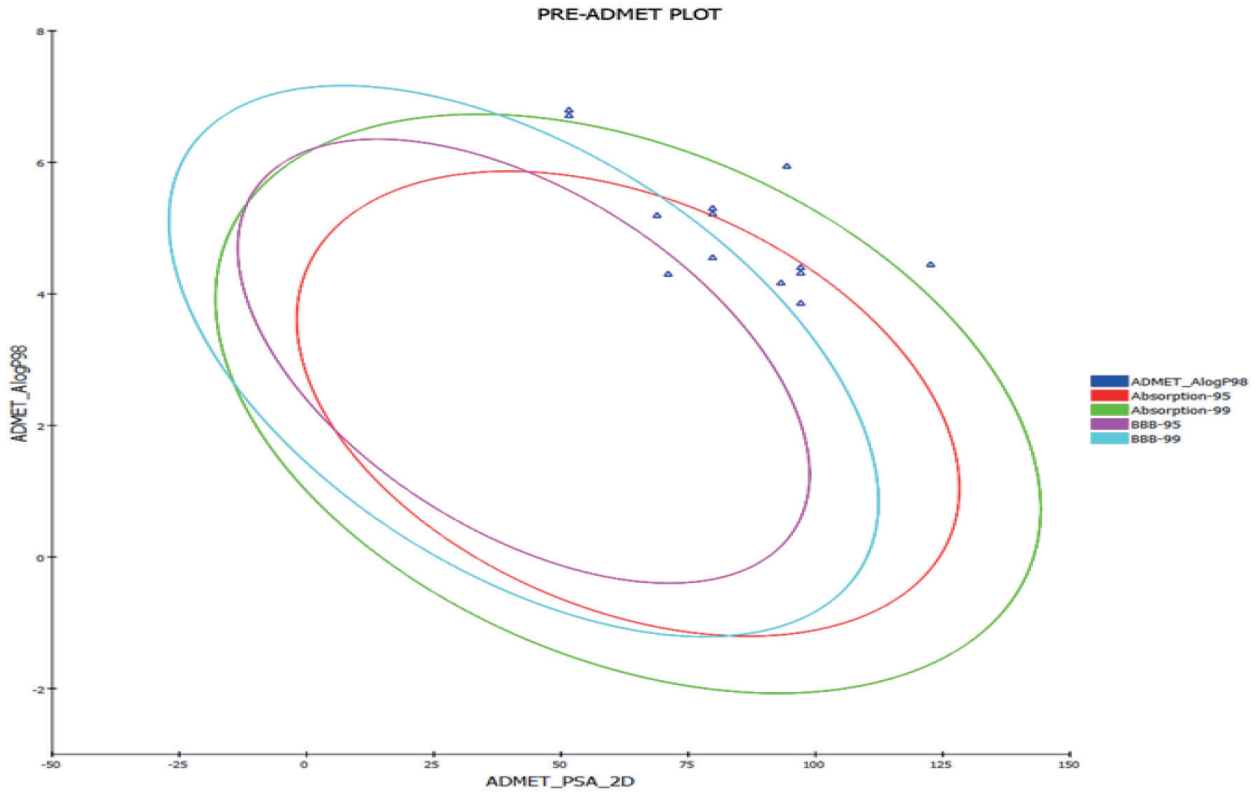

Figure 6. Predicted ADMET results for the synthesized (NF) derivatives.

Table 5. Spatial distribution of molecular orbitals for the tested ligands.

Comp.	Total Energy (kcal/mol)	Binding Energy (kcal/mol)	HOMO Energy (kcal/mol)	LUMO Energy (kcal/mol)	Dipole moment. Debye	Band Gap Energy (kcal/mol)
3A	-4053.52	-9.407	-0.198	-0.111	1.697	0.087
4C	-3684.32	-9.965	-0.2136	-0.156	3.4869	0.057
4D	-2008.56	-9.6656	-0.2089	-0.1430	3.4782	0.0659
5B	-1932.5	-9.174	-0.211	-0.1531	0.7232	0.0579
Crystal-Ligand (1YWN)	-1921.4	-10.226	-0.190	-0.153	4.082	0.037
Erlotinib (4HJO)	-1305.6	-10.051	-0.1882	-0.092	2.323	0.0962

of -4053.52, -3684.32, -2008.56, and -1921.4 kcal/mol, respectively. Such findings revealed that compounds **3A** and **4C** possess the highest total energy, indicating the high chance for drug-receptor complex formation. Correspondingly, compound **4C** had the highest dipole moment value of 3.486 (debye), referring to the high possibility of compound **4C** interacting with the target receptor: VEGFR tyrosine kinase. In a similar manner, compound **4C** had a low gap energy value of 0.0576 kcal/mol, indicating the high reactivity of such a compound to interact with the target macromolecule. Moreover, compounds **5B** and Erlotinib had total energy values of -1932.5 and -1305.6; dipole moment values of 0.7232 and 2.323 (debye), and the gap energy value of 0.0579, and 0.0962 kcal/mol, respectively. That indicates that compound **5B** has a high chance for drug-receptor complex formation with EGFR tyrosine kinase.

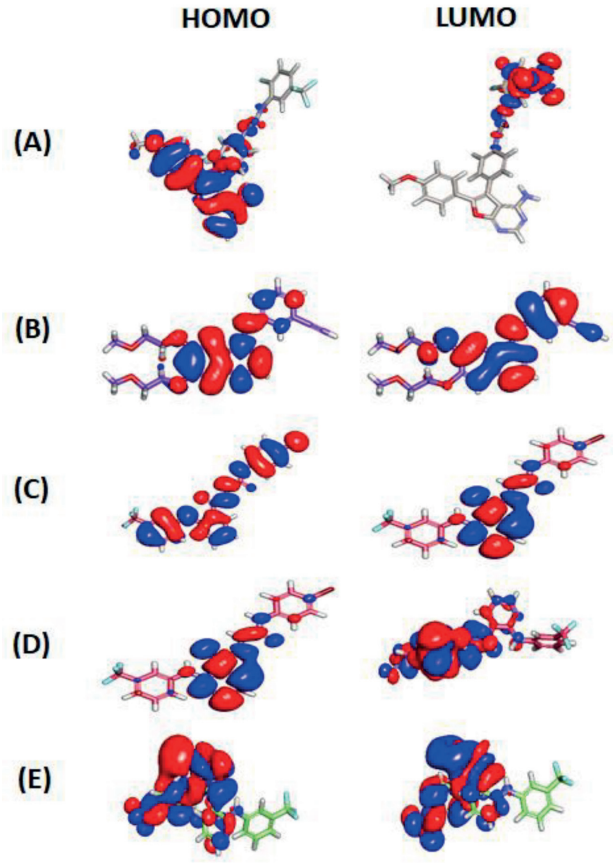

Figure 7. Spatial distribution of molecular orbitals for (A) Crystal-Ligand (1YWN), (B) ligand Erlotinib (4HJO), (C) ligand **3A**, (D) ligand **4D**, and (E) ligand **5C**.

Molecular dynamics (MD) simulations

Molecular dynamics (MD) simulations were carried out to compare the binding stability of the tested compounds. After doing the molecular docking, ligand **4D** showed more stability, binding by more hydrogen bonds than other ligands. An MD simulation has been done to confirm its stability, which revealed that ligand **4D** showed a good RMSD value along of 100 ns MD, the target protein showed a RMSD value of 2.7°A, while the complex exhibited a RMSD value of 3.7°A. An acceptable range is around 4°A. This complex was shown to be stable in a 100 ns MD simulation (Fig. 8).

Biological study

The effects of the tested compounds on Hep G2 and A549 cancer cell proliferation

The *in vitro* anti-proliferative effects of the 11 tested compounds (**3A-6**) were evaluated by the MTT assay (Suppl. material 1: Figs S1, S2). The results presented in Table 6 show that all of the tested compounds exhibited cytotoxicity against the two cancer cell lines. Additionally, the results show that compound **4C** was the most cytotoxic compound resulting in IC_{50} concentration of 4.62 µM against Hep G2. Accordingly, this compound was chosen for the subsequent biological investigation.

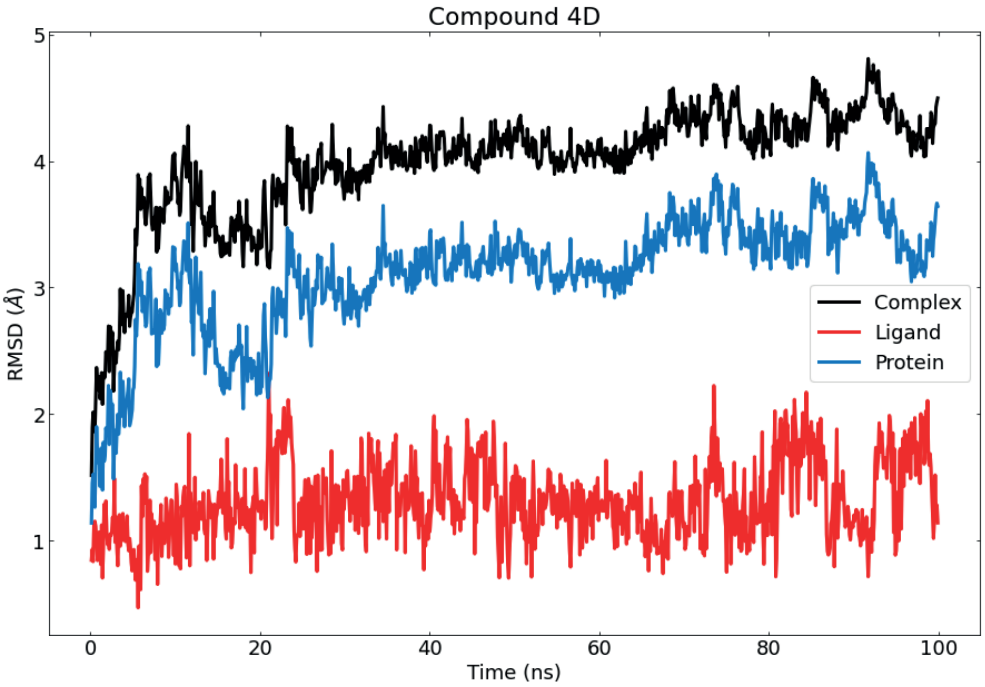

Figure 8. RMSD value of compound **4D** in MD runs. Red: Ligand **4D**, blue: Target protein, black: Complex of ligand **4D** and target protein.

Table 6. *In vitro* anti-proliferative activities of the tested compounds against Hep G2 and A549 cancer cell lines. Data shown is the average IC_{50} values in µM of three independent experiments performed in triplicates.

Compound	IC_{50}/HepG2	IC_{50}/A549
3A	9.68	8.56
3B	23.71	27.83
3C	16.06	21.05
4A	19.52	23.13
4B	8.19	8.59
4C	**4.62**	10.01
4D	11.65	19.52
5A	26.09	14.80
5B	7.10	**5.24**
5C	43.91	45.08
6	18.69	12.27

Furthermore, the selectivity of compound 4C against cancer cells was assessed. The cytotoxicity of compound 4C was tested against the normal cell line WI-38 lung fibroblasts, and the IC50 calculated for this compound against WI-38 cells was 33.42 µM (Suppl. material 1: Fig. S1). A compound/drug is considered strongly cytotoxic if its IC50 is between 10-100 µg/mL, and since compound 4C IC50 was 4.62 µM = 15.45 µg/mL (molecular weight = 465.88 g/mol), it is a strong cytotoxic compound. Additionally, compound 4C is cancer-selective since its selectivity index (SI) is larger than 3 (SI= IC50 non-cancer cells/IC50 cancer cells = 33.42/4.62= 7.2) (Weerapreeyakul et al., 2012) (Indrayanto, G., Putra, G.S., Suhud, 2021).

Compound 4C-treated Hep G2 hepatocyte carcinoma cells exhibit disruption in cell cycle progression

Control and 48 h compound **4C**-treated (at the IC_{50} concentration) Hep G2 cells were stained with propidium iodide (PI), and the distribution (%) of cells in each phase of the cell cycle (Sub-G1, G1, S, and G2/M) was determined by flow cytometry (Fig. 9). The results shown in Table 7, indicate that treated cells were arrested at the S and G2/M phases (56.2% and 80.2% increase, as compared to control

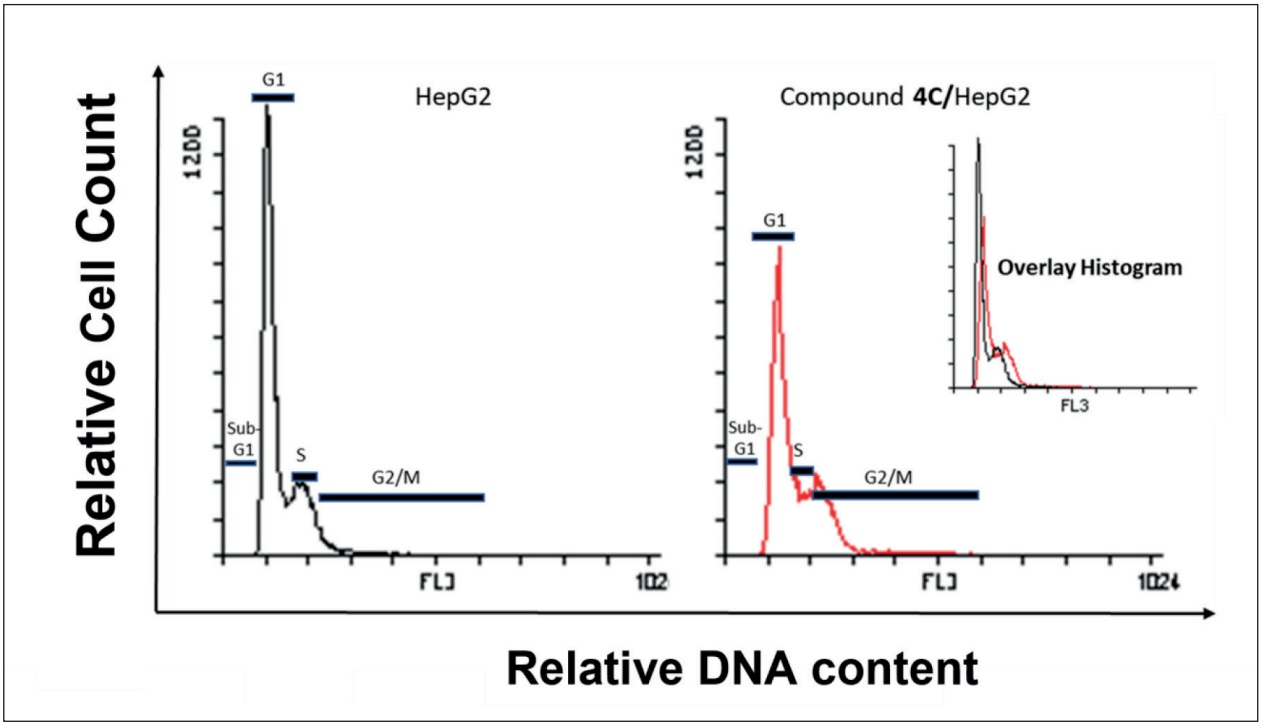

Figure 9. Flow cytometric analysis of cell cycle phases in control and compound **4C**-treated Hep G2 hepatocyte carcinoma cells. Hep G2 Cells were treated with 4.62 µM (IC_{50} value) of compound **4C** for 48 h, stained with PI and subjected to flow cytometry.

Table 7. Distribution of control and compound **4C**-treated Hep G2 cells in the different phases of the cell cycle. Values are given as mean ± SEM. *p < 0.05, **p < 0.01, as compared to control cells.

	% Sub-G1	% G1	% S	% G2/M
Control	0.57 ± 0.30	58.84 ± 3.91	23.76 ± 2.90	16.83 ± 1.41
Compound 4C-treated	0.78 ± 0.13	31.78 ± 0.97**	37.12 ± 1.31*	30.32 ± 1.09**

Table 8. The cytotoxicity of compound **4C** against Hep G2 hepatocyte carcinoma cells is attributed to apoptosis not necrosis. Values are given as mean ± SEM. ****p < 0.0001, as compared to control Hep G2 cells.

	% Viable	%Early apoptosis	% Late apoptosis	% Necrosis
Control	92.94 ± 1.44	6.17 ± 1.59	0.78 ± 0.17	0.11 ± 0.03
Compound 4C treated	46.59 ± 1.56	51.86 ± 1.69****	1.42 ± 0.20	0.13 ± 0.02

cells, respectively), while the percentage of treated cells in the G1 phases was reduced 46%, as compared to control cells. (Table 7). Cell cycle arrest at the S and G2 cell cycle phases has been reported previously for other drugs which caused DNA damage during DNA replication and thus resulted in S phase extension, and if this damage was not repaired, the cell cycle was arrested at the G2 phase (Orren et al. 1997), (Gunsedogan et al. 2014).

The cytotoxicity of compound 4C against Hep G2 hepatocyte carcinoma cells is attributed to apoptosis

Since compound **4C** (and the other compounds as well) caused cytotoxicity, we aimed to investigate if compound **4C** caused cell killing by inducing apoptosis and/or necrosis. Control and treated Hep G2 cells were fixed, stained with PI and annexin V-FITC, and subjected to flow cytometry (Fig. 10A). Data presented in Table 8, suggest that compound **4C** reduced the percentage of viable Hep G2 cells, by inducing early apoptosis.

To confirm compound 4C induction of apoptosis, the mRNA levels of 4 apoptosis markers [p53, BAX (pro-apoptosis), Bcl-2 (anti-apoptosis), and caspase-3) were measured by qRT-PCR and the results are shown in Fig. 10B. The results indicate that p53, BAX and caspase-3 mRNA levels in compound 4C-treated Hep G2 cells were up regulated significantly, as compared to control cells, while the mRNA level of Bcl-2 was reduced, although insignificantly (Fig. 10B). The upregulation of BAX and down-regulation of Bcl-2 in compound 4C-treated Hep G2 cells indicate that compound 4C caused cell killing by inducing the intrinsic apoptotic pathway (Adams and Cory, 2007).

Compound 4C targets VEGFR-2 kinase and compound 5B targets EGFR kinase

The results of the molecular docking studies presented in the current work classified the tested compounds into 2 groups, a group that has the potential to target vascular endothelial growth factor receptor (VEGFR; compounds **3A, 3B, 3C, 4A, 4B, 4C,** and **4D**), while the second group has the potential to target epithelial growth factor receptor (EGFR; **5A, 5B, 5C**, and **6**). Since compounds **4C** and **5B** achieved the lowest IC_{50} concentrations (Table 9), they were chosen to test for their VEGFR and EGFR inhibition activities (Fig. 11).

The results shown in Table 9 indicate that compound **4C** was able to inhibit VEGFR-2 kinase activity and its EC_{50} (77.23 nM) was comparable to that of Sorafenib (57.75 nM), a standard VEGFR-2 kinase inhibitor (htt-

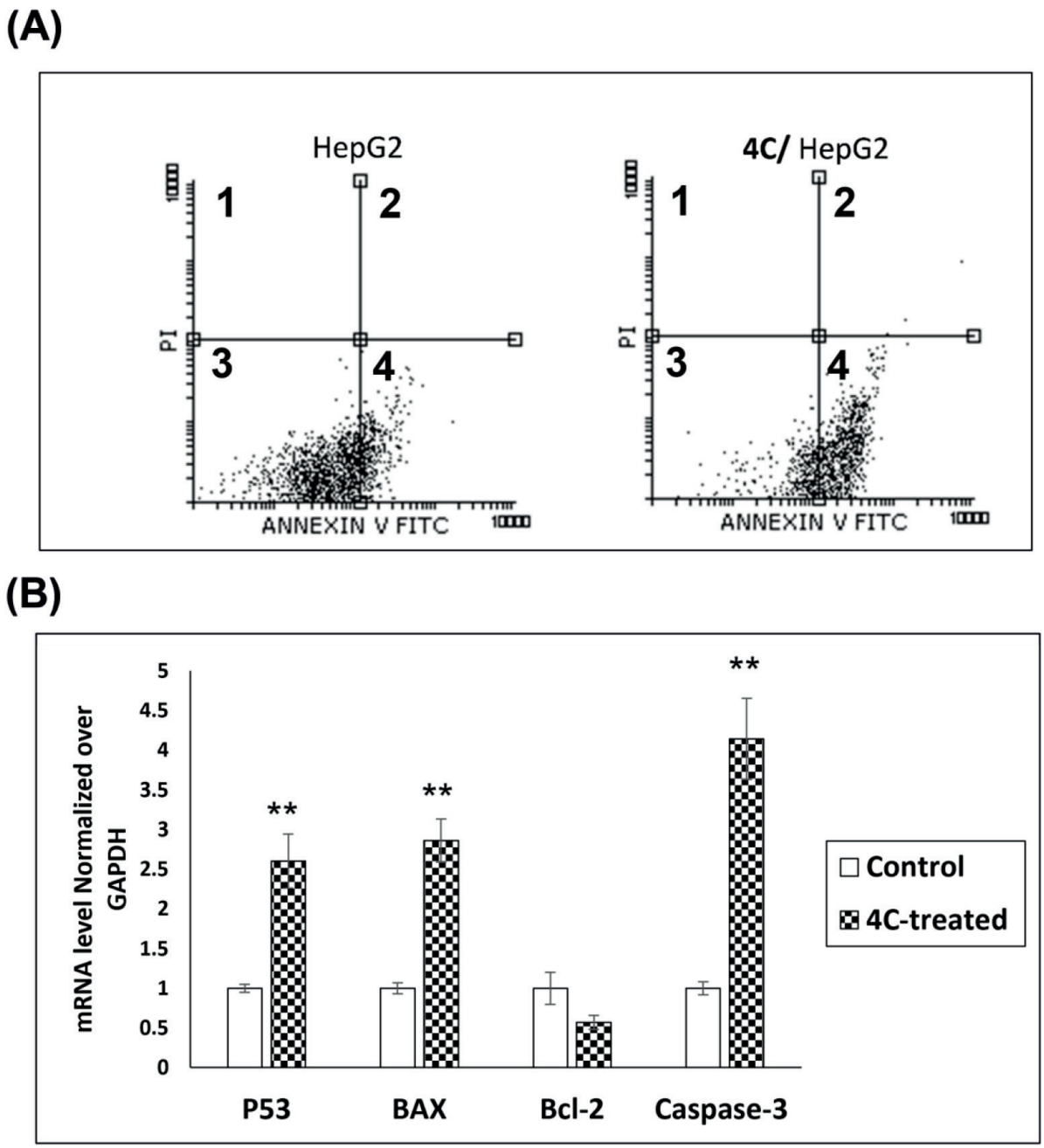

Figure 10. Cytotoxicity of compound **4C** is attributed to apoptosis not necrosis. **A**) Hep G2 cells were treated with compound **4C** (4.62 μM) for 48 h, harvested, stained with AnnexinV-FITC/propidium iodide (PI), and analyzed for apoptosis (early: bottom right corner negative PI/positive annexin V; late: top right corner positive PI/positive annexin V) versus necrosis (top left corner positive PI/negative annexin V) using flow cytometry, **B**) mRNA level analysis of p53, BAX, Bcl-2, and caspases-3 genes, normalized over GAPDH, in control and compound **4C**-treated Hep G2 cells. Values are given as mean ± SEM of three independent experiments. *p < 0.05, **p < 0.01 as compared to control cells.

ps://pubchem.ncbi.nlm.nih.gov/compound/Sorafenib). On the other hand, compound **5B** was able to inhibit EGFR kinase activity resulting in EC_{50} value of 25.38 nM which was comparable to that of Erlotinib (9.91 nM), a standard EGFR kinase inhibitor (https://pubchem.ncbi.nlm.nih.gov/compound/Erlotinib).

3D-QSAR model generation and validation

A training set of 32 FDA approved VEGFR-2 tyrosine kinase inhibitors of known activity with IC_{50} values ranging from 0.035 to 1.2 M and a training set of 16 FDA approved EGFR tyrosine kinase inhibitors of known activity with IC_{50} values ranging from 0.5 to 37 M were collected from the Selleck hem library [https://www.selleckchem.com/subunits/VEGFR2_VEGFR_selpan.html]. The structures of these VEGFR-2 inhibitors were first drawn in Chem BioDraw Ultra 17 and saved in MDL-SD file format. The saved file was then opened by the Discovery Studio 2016 software. The ligand prepare protocol was used to prepare the structures, and the force fields (CHARMM and

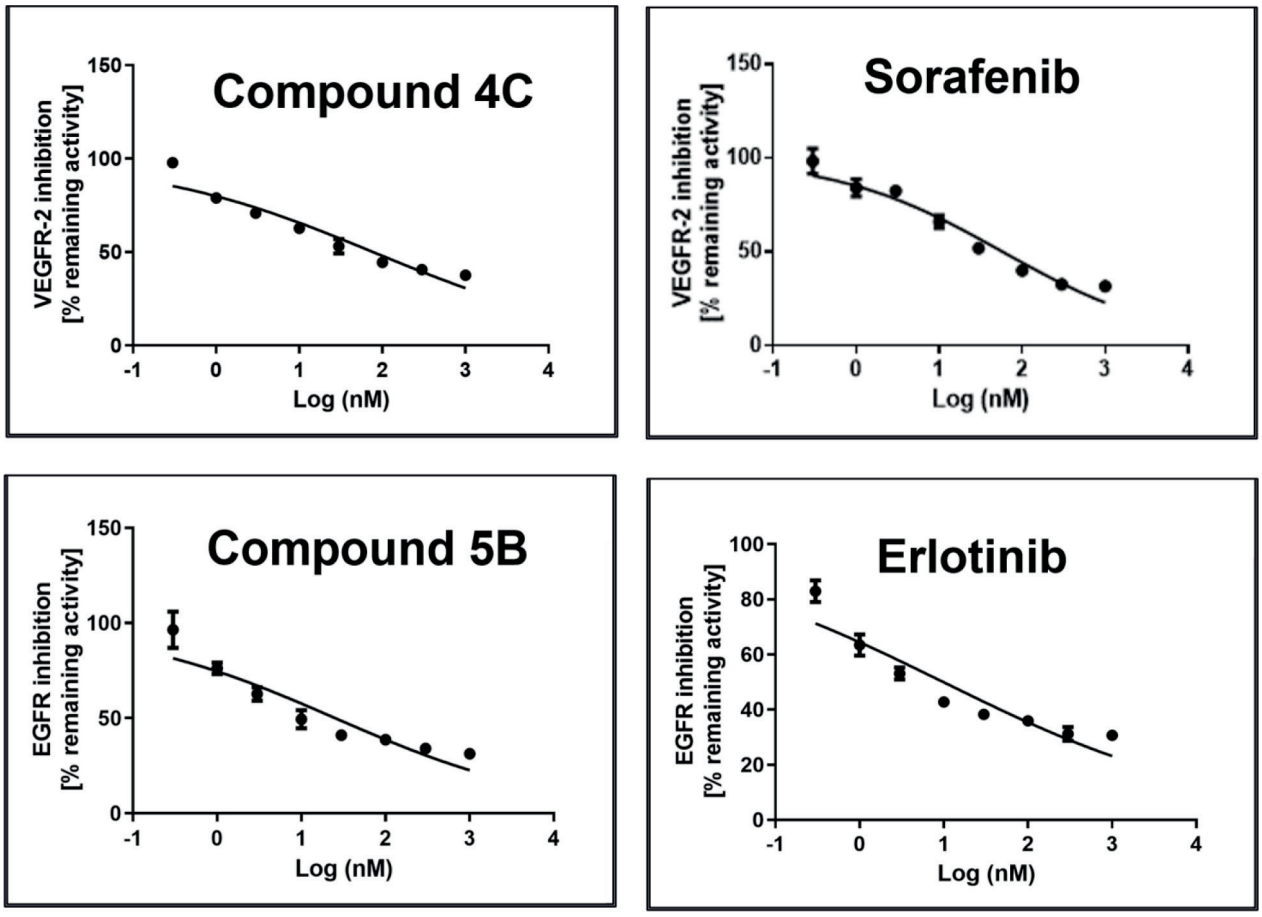

Figure 11. *In vitro* receptor-tyrosine kinase inhibitory activity of compound **4C** and compound **5B**.

Table 9. EC_{50} values (nM) of the tested compounds (**4C** and **5B**) and standard compounds (Sorafenib and Erotinib) against EGFR or VEGFR Kinases. The experiment was performed three times.

Compound	EGFR kinase	VEGFR-2 kinase
4C	–	77.23
Sorafenib	–	57.75
5B	25.38	–
Erlotinib	9.91	–

MMFF94) were used. The Grid Based Temp Model protocol was also used to generate a 3D QSAR model after the ligands were prepared. To determine the impact of substitutes on anticancer activity, quantitative structure-activity relationships (QSAR) were investigated. A Grid Based Temp Model (GBTM) analysis was used to generate models using a training set of 32 FDA-approved VEGFR-2 inhibitors, and a training set of 16 FDA-approved EGFR TK inhibitors. Data on anticancer activity was transformed from IC_{50} to PIC_{50} values (i.e., -logIC_{50}), and used as dependent variables in QSAR studies. The generated QSAR model was depicted graphically by scattering plots of anticipated anticancer activity against VEGFR-2 versus experimental values for the training data set compounds, as shown in (Fig. 12), and (Fig. 13).

3D-QSAR Validation VEGFR-2 TK

The validity of our QSAR model was proven by leave-one-out (LOO) internal validation (r^2 = 0.829).

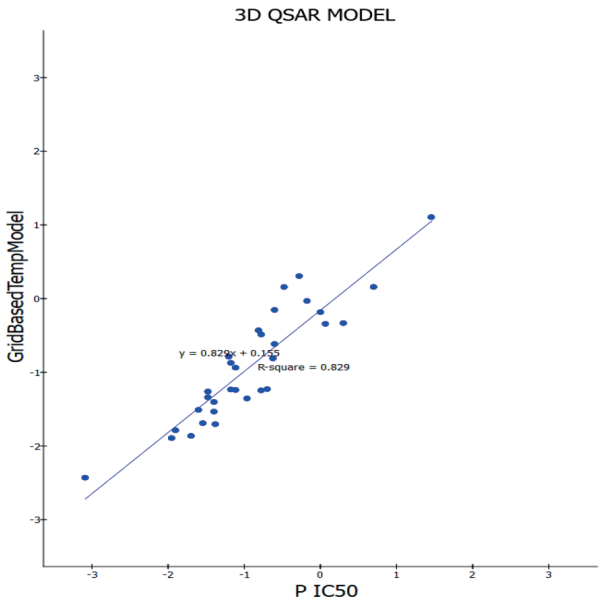

Figure 12. Predicted (Y-axis) versus experimental anticancer activity (X-axis –(PIC_{50})) of the training set compounds against VEGFR-2 tyrosine kinase target site.

Cross-validation was also employed where q^2, which is equivalent to r^2 (pred), was 0.829. The increased value of q^2 greater than 0.5 reveals the validity of a QSAR model (Suppl. material 1: Table S1). Moreover, measuring the residuals between the experimental and the predic-

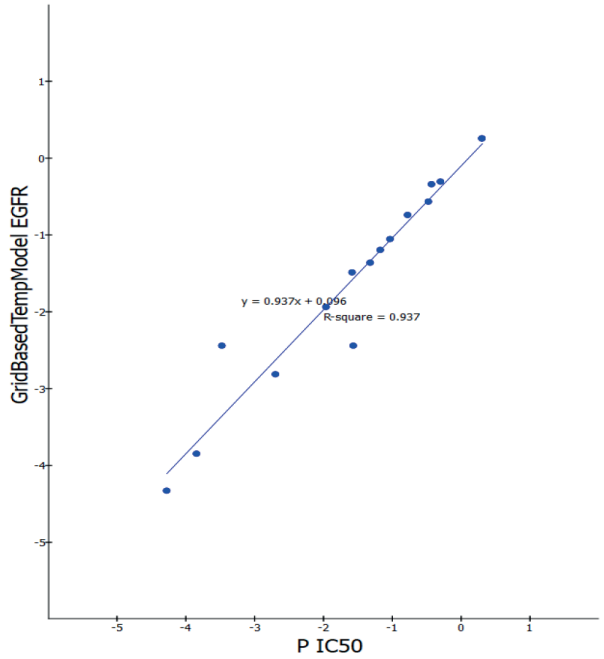

Figure 13. Predicted (Y axis) versus experimental anticancer activity (X axis -PIC50) of the training set compounds against EGFR tyrosine kinase target site.

ted activities of the training set gave an additional QSAR model validation, where the predicted activities by the established QSAR model were very close to those experimentally assessed, indicating that this model could be applied for anti-cancer prediction of other effective analogues (Suppl. material 1: Table S2). Finally, the synthesized compounds were tested by the generated QSAR model. It was observed that the predicted EC_{50} is very close to the experimental EC_{50} against the VEGFR-2 target site (Table 10).

Table 10. Comparison between the experimental IC_{50} and the predicted IC_{50} of few synthesized compounds against VEGFR-2 tyrosine kinase obtained by QSAR model.

Compound	Experimental IC_{50} (nM)	Predicted IC_{50} (nM)
3A	NA not tested	87.53
3b	NA not tested	72.33
3c	NA not tested	61.65
4A	NA not tested	51.99
4B	99.91	72.02
4C	77.23	69.12
4D	NA not tested	64.56

3D QSAR Validation EGFR TK

The validity of our QSAR model was proven by leave-one-out (LOO) internal validation (r^2 = 0.937). Cross-validation was also employed where q^2, which is equivalent to r^2 (pred), was 0.937. The increased value of q^2 greater than 0.5 reveals the validity of a QSAR model. Measuring the difference between the experimental and predicted activities of the training set gave an additional validation of the QSAR model. The activities predicted by the established QSAR model were very close to those tested experimentally, which showed that this model could be used to predict the anti-cancer effects of other effective analogues (Table 11). The synthesized compounds were tested using a generated QSAR model, and the predicted IC_{50} was found to be very close to the experimental IC_{50} against the EGFR tyrosine kinase target site.

Table 11. Comparison between the experimental and predicted anticancer activity of the test set compounds (synthesized) against EGFR tyrosine kinase obtained by QSAR model.

Comp.	Experimental IC_{50} (nM)	Predicted IC_{50} (nM)
5A	NA	38.90
5B	**25.38**	18.28
5C	NA	70.64
6	**43.44**	36.30

SAR study

Study of the Structure-Activity Relationships (SAR) of the new compounds revealed several common findings. The presence of an aryl or a heteroaryl fragment attached *via* the hydrophilic linker is crucial to the anticancer activity. Accordingly, compounds that have a hydrazine-1-carbothioamide moiety showed good activity, compared with those containing a hydrazine-1-carboxamide moiety (IC_{50} range = 8.59–23.13 μM, compared with 8.56–27.83 μM), respectively. According to the terminal hydrophobic moiety, compounds **3A, 3B, and 3C** contain hydrazine-1-carboxamide, but are different in the terminal substitution at the hydrophobic part. The IC_{50} of the derivatives containing bromo (**3A),** and fluoro (**3C**) groups, was higher than that of derivatives containing chloro **(3B**) group. According to the derivatives that contain hydrazine-1-carbothioamide, compounds (**4A, 4B, 4C, and 4D),** chloro derivative (**4C**), had the highest IC_{50} compared with bromo (**4B**), nitro (**4D**), and unsubstituted (**4A**) aromatic derivatives, (Fig. 14).

The SAR of the new compounds **(5A, 5B, 5C,** and **6)** revealed several common findings. The presence of an aryl or a heteroaryl fragment attached *via* the hydrophilic linker is crucial to the anticancer activity. According to compounds (**5A, 5B, 5C**, and **6**), chloro derivative (**5B**) is better than bromo (**5A**) derivative, and nitro derivative (**5C**), which indicates the activity is enhanced by increasing electro negativity (Fig. 15).

Conclusion

A series of niflumic acid derivatives (**3A–6**) have been successfully synthesized, and their chemical structures were confirmed using FT-IR, ^{1}H, and ^{13}C-NMR, and MS. The molecular docking studies, and MTT assay for the tested compounds showed a high correlation between the expected

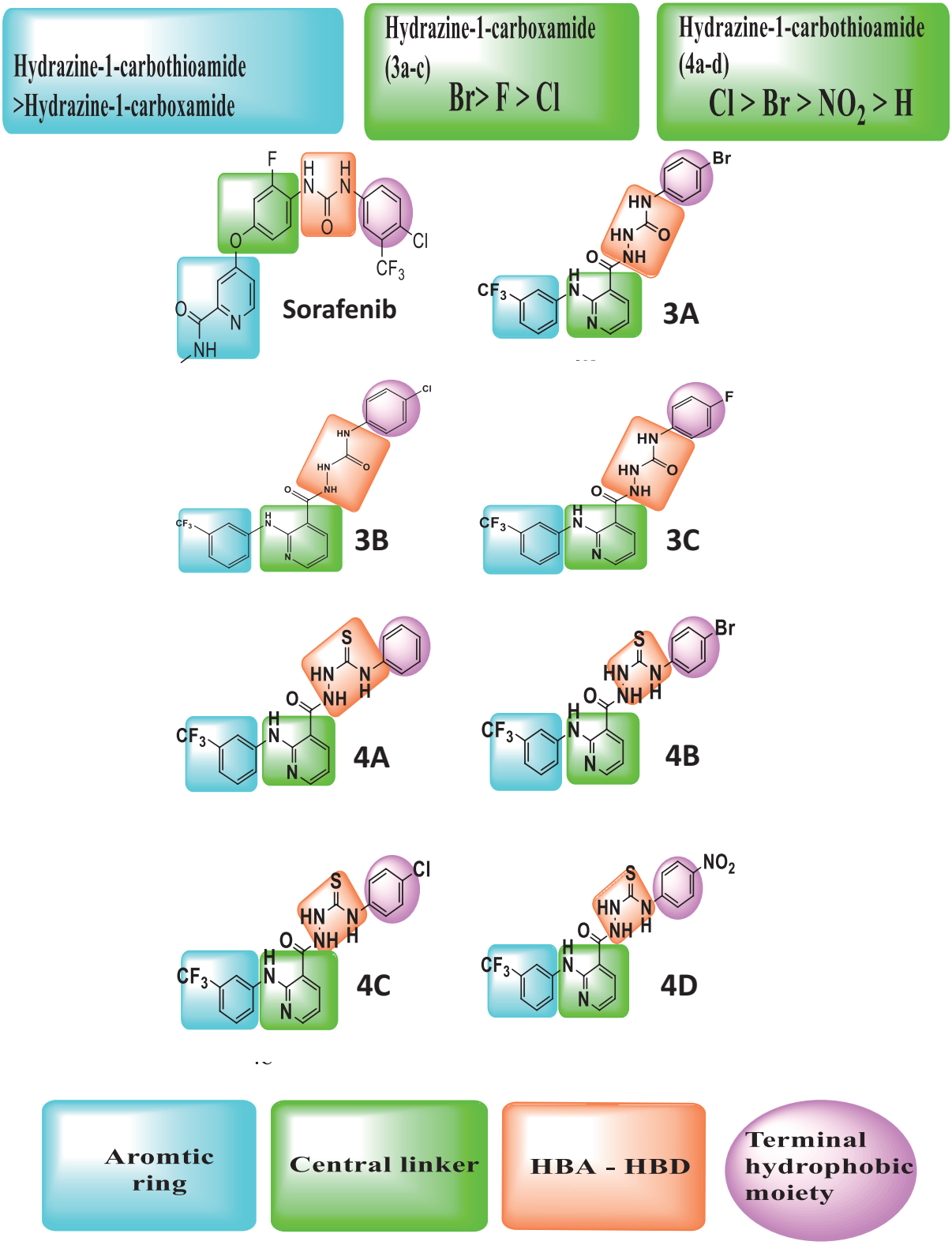

Figure 14. SAR studies revealed common features of compounds predicted as VEGFR-2 tyrosine kinase inhibitors.

results from the molecular modeling and the wet-lab biological evaluations, which indicated high selectivity against the VEGFR, and EGFR tyrosine kinase target sites. Additionally, *in silico pre*-ADMET study showed that all tested compounds have low CNS side effects, and a carcinogenicity score close to zero. The newly synthesized niflumic acid derivatives are potent anticancer agents which inhibit cell proliferation by inhibiting VEGFR tyrosine kinase or EGFR tyrosine kinase activity, which leads to cell cycle arrest, which in turn induces apoptosis, leading to cancer cell killing (Fig. 16).

Figure 15. SAR studies revealed common features of compounds predicted as EGFR tyrosine kinase inhibitors.

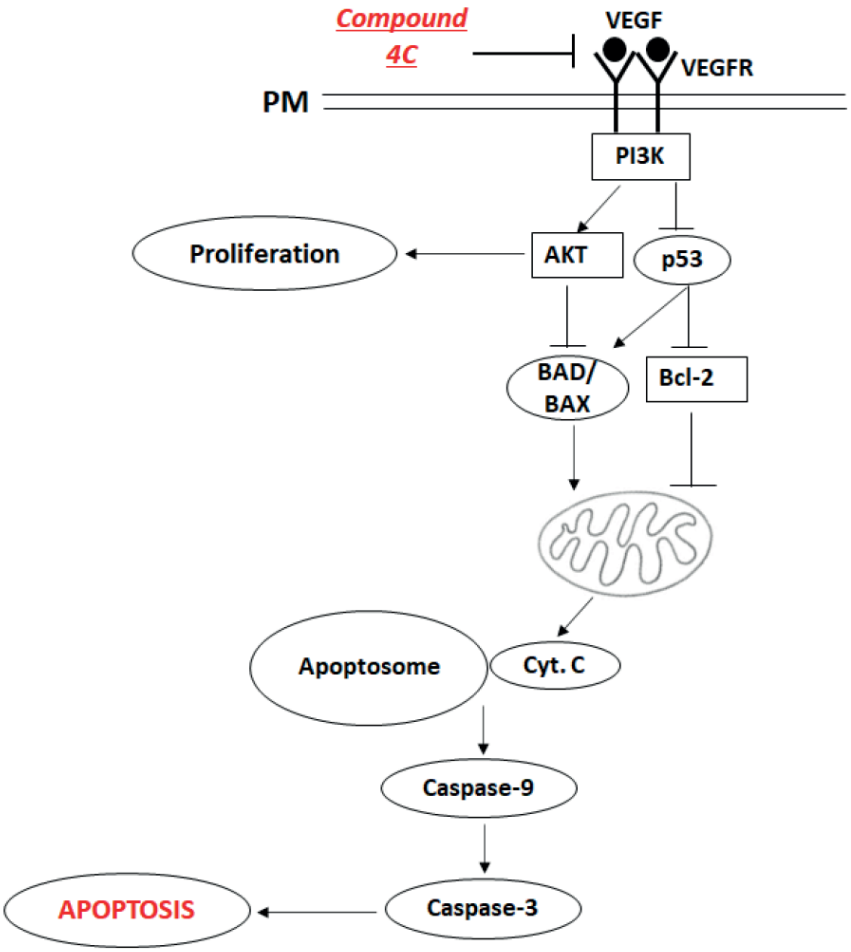

Figure 16. A model explaining the signaling pathway downstream of compound 4C leading to apoptosis.

Conflict of Interest

The authors declare that there is no conflict of interest.

Acknowledgement

The authors are grateful to the Department of Pharmaceutical Chemistry, College of Pharmacy, University of Baghdad, Iraq, for supporting the current work.

References

Abbas AH, Mahmoo, AAR, Tahtamouni LH, Al-Mazaydeh ZA, Rammaha MS, Alsoubani F, Al-Bayati RI (2021) A novel derivative of picolinic acid induces endoplasmic reticulum stress-mediated apoptosis in human non-small cell lung cancer cells: synthesis, docking study, and anticancer activity. Pharmacia 68(3): 679–692. https://doi.org/10.3897/pharmacia.68.e70654

Adams JM, Cory S (2007) Bcl-2-regulated apoptosis: mechanism and therapeutic potential. Current Opinion in Immunology 19(5): 488–496. https://doi.org/10.1016/j.coi.2007.05.004

Al-Abodi A, Al-Fartusie F, Al-Fartusie F (2005) Synthesis of new nicotinic acid derivatives and studying their effects on Cho Hinesteeas Enzywr Activity. Journal of Techniques 18(1): 57–66.

Al-Bayati AI, Razzak Mahmood AA, Al-Mazaydeh ZA, Rammaha MS, Al-bayati RI, Alsoubani F, Tahtamouni LH (2021) Synthesis, Docking Study, and *in vitro* anticancer evaluation of new flufenamic acid derivatives. Pharmacia 68(2): 449–461. https://doi.org/10.3897/pharmacia.68.e66788

Al AA, Hassa AA, Makhlou MM, Bräse S (2020) Chemistry and biological activities of 1,2,4-triazolethiones-antiviral and anti-infective drugs. Molecules 25(13): e3036. https://doi.org/10.3390/molecules25133036

Amadio M, Govoni S, Pascale A (2016) Targeting VEGF in eye neovascularization: What's new?: A comprehensive review on current therapies and oligonucleotide-based interventions under development. Pharmacological Research 103 253–269. https://doi.org/10.1016/j.phrs.2015.11.027

Bhatt AN, Mathur R, Farooque A, Verma,A, Dwarakanath BS (2010) Cancer biomarkers - Current perspectives. Indian Journal of Medical Research 132(8): 129–149.

Bulut N, Kocyigit UM, Gecibesler IH, Dastan T, Karci H, Taslimi P, Durna Dastan S, Gulcin I, Cetin A (2018) Synthesis of some novel pyridine compounds containing bis-1,2,4-triazole/thiosemicarbazide moiety and investigation of their antioxidant properties, carbonic anhydrase, and acetylcholinesterase enzymes inhibition profiles. Journal of Biochemical and Molecular Toxicology 32(1): 2–11. https://doi.org/10.1002/jbt.22006

Genheden S, Ryde U (2012) Comparison of end-point continuum-solvation methods for the calculation of protein-ligand binding free energies. Proteins: Structure, Function and Bioinformatics 80(5): 1326–1342. https://doi.org/10.1002/prot.24029

Günesdogan U, Jäckle H, Herzig A (2014) Histone supply regulates S phase timing and cell cycle progression. ELife 3: e02443. https://doi.org/10.7554/eLife.02443

Heindel ND, Reid JR (1980) 4-Amino-3-mercapto-4*H*-1,2,4-triazoles and propargyl aldehydes: A new route to 3-R-8-aryl-1,2,4-triazolo[3,4-b]-1,3,4-thiadiazepines. Ind Journal of Heterocyclic Chemistry 17(5): 1087–1088. https://doi.org/10.1002/jhet.5570170547

Hmood KS, Ammar ARMK, Al-Bayati RI, Saleh AM (2021) Synthesis, and anti-tumor evaluation of some new Flurbiprofen derivatives against MCF-7 and WRL-68 cell lines. Indonesian Journal of Pharmacy 32(1): 17–34. https://doi.org/10.22146/ijp.730

Holla B, Kalluraya B, Sridhar K, Drake E, Thomas L, Bhandary K, Levine M (1994) Synthesis, structural characterization, crystallographic analysis and antibacterial properties of some nitrofuryl triazolo[3,4-b]-1,3,4-thiadiazines. European Journal of Medicinal Chemistry 29(4): 301–308. https://doi.org/10.1016/0223-5234(94)90100-7

Husain A, Rashid M, Mishra R, Parveen S, Shin DS, Kumar D (2012) Benzimidazole bearing oxadiazole and triazolo-thiadiazoles nucleus: Design and synthesis as anticancer agents. Bioorganic and Medicinal Chemistry Letters 22(17): 5438–5444. https://doi.org/10.1016/j.bmcl.2012.07.038

Indrayanto G, Putra GS, Suhud F (2021) Chapter Six - Validation of in-vitro bioassay methods: Application in herbal drug research. Elsevier 46: 273–307. https://doi.org/10.1016/bs.podrm.2020.07.005

Jiang X, Liu Y, Zhang G, Lin S, Wu J, Yan X, Ma Y, Ma M (2020) Aloe-Emodin Induces Breast Tumor Cell Apoptosis through Upregulation of miR-15a / miR-16-1 That Suppresses BCL2. Evidence-Based Complementary and Alternative Medicine 2020: e5108298. [10 pp] https://doi.org/10.1155/2020/5108298

Khodapasand E, Jafarzadeh N, Farrokhi F, Kamalidehghan B, Houshmand M (2015) Is Bax/Bcl-2 ratio considered as a prognostic marker with age and tumor location in colorectal cancer? Iranian Biomedical Journal 19(2): 69–75. https://doi.org/10.6091/ibj.1366.2015

Mirza AZ, Althagafi II, Shamshad H (2019) Role of PPAR receptor in different diseases and their ligands: Physiological importance and clinical implications. European Journal of Medicinal Chemistry 166: 502–513. https://doi.org/10.1016/j.ejmech.2019.01.067

Mosmann T (1983) Rapid colorimetric assay for cellular growth and survival: application to proliferation and cytotoxicity assays. Journal of Immunological Methods 65(1-2):55-63. http://doi: 10.1016/0022-1759(83)90303-4

Narayanan R, Kuppermann BD, Jones CKPR (2006) Thermo-responsive hydro gels for intravitreal injection and biomolecule release. 104 pp.

Nederlof A (1963) The preparation and reactions of some rhodanines. Recueil Des Travaux Chimiques Des Pays-Bas 82(1): 75–89. https://doi.org/10.1002/recl.19630820109

Nunez R (2001) DNA Measurement and Cell Cycle Analysis by Flow Cytometr. Current Issues in Molecular Biology 3(3): 67–70.

Oda K, Matsuoka Y, Funahashi A, Kitano H (2005) A comprehensive pathway map of epidermal growth factor receptor signaling. Molecular Systems Biology 1(1): 2005–0010. https://doi.org/10.1038/msb4100014

Orren DK, Petersen LN, Bohr VA (1997) Persistent DNA damage inhibits S-phase and G2 progression, and results in apoptosis. Molecular Biology of the Cell 8(6): 1129–1142. https://doi.org/10.1091/mbc.8.6.1129

Pandey AK, Singhi EK, Arroyo JP, Ikizler TA, Gould ER, Brown J, Beckman JA, Harrison DG, Moslehi J (2018) Mechanisms of VEGF (vascular endothelial growth factor) inhibitor-associated hyperten-

sion and vascular disease. Hypertension 71(2): 1524–4563[E1–E8]. https://doi.org/10.1161/HYPERTENSIONAHA.117.10271

Peluffo MC, Young KA, Stouffer RL (2005) Dynamic expression of caspase-2, -3, -8, and -9 proteins and enzyme activity, but not messenger ribonucleic acid, in the monkey corpus luteum during the menstrual cycle. Journal of Clinical Endocrinology and Metabolism 90(4): 2327–2335. https://doi.org/10.1210/jc.2004-2214

Pozarowski P, Darzynkiewicz Z (2014) Analysis of cell cycle by flow cytometry methods in molecular biology 2: 301–311. https://doi.org/10.1385/1-59259-811-0

Rashid M, Husain A, Mishra R (2012) Synthesis of benzimidazoles bearing oxadiazole nucleus as anticancer agents. European Journal of Medicinal Chemistry 54: 855–866. https://doi.org/10.1016/j.ejmech.2012.04.027

Rubio RG, Adamis AP (2015) Ocular angiogenesis: Vascular endothelial growth factor and other factors. Developments in Ophthalmology 55: 28–37. https://doi.org/10.1159/000431129

Seidel T, Wieder O, Garon A, Langer T (2020) Applications of the pharmacophore concept in natural product inspired drug design. Molecular Informatics 39(11): e2000059. https://doi.org/10.1002/minf.202000059

Seshacharyulu P, Ponnusamy MP, Haridas D, Jain M, Ganti AK, Batra SK (2012) Targeting the EGFR signaling pathway in cancer therapy. Expert Opinion on Therapeutic Targets 16(1): 15–31. https://doi.org/10.1517/14728222.2011.648617

Shaker RM (2006) Synthesis of polyfunctionally substituted benzo[5,6]chromeno[4,3,2-de][1,6] naphthyridines and 5H-benzo[5,6]chromeno[3,4-c]pyridines. Arkivoc 14: 59–67. https://doi.org/10.3998/ark.5550190.0007.e09

Shibuya M (2011) Vascular endothelial growth factor (VEGF) and its receptor (VEGFR) signaling in angiogenesis: A crucial target for anti- and pro-angiogenic therapies. Genes and Cancer 2(12): 1097–1105. https://doi.org/10.1177/1947601911423031

Wang E, Sun H, Wang J, Wang Z, Liu H, Zhang JZH, Hou T (2019) End-point binding free energy calculation with MM/PBSA and MM/GBSA: Strategies and applications in drug design [Review-article]. Chemical Reviews 119(16): 9478–9508. https://doi.org/10.1021/acs.chemrev.9b00055

Weerapreeyakul N, Nonpunya A, Barusrux S, Thitimetharoch T (2012) Evaluation of the anticancer potential of six herbs against a hepatoma cell line. Chinese Medicine 7: e15. https://doi.org/10.1186/1749-8546-7-15

Yarden Y, Schlessinger J (1987) Epidermal growth factor induces rapid, reversible aggregation of the purified epidermal growth factor receptor. Biochemistry 26(5): 1443–1451. https://doi.org/10.1021/bi00379a035

Zhang X, Wang Q, Xu Y, Wang B, Jia C, Wang L, Sun H, Zhao H, Wang Z, Zou Q, Sun S, Zhang L (2019) LncRNA PCAT19 negatively regulates p53 in non-small cell lung cancer. Oncology Letters 18(6): 6495–6800. https://doi.org/10.3892/ol.2019.11041

Supplementary material 1

Figures S1, S2, Tables S1, S2

Authors: Yahya Yaseen, Ammar Kubba, Wurood Shihab, Lubna Tahtamouni

Data type: Doc file

Explanation note: **Figure S1.** The MTT assay results of the 11 tested compounds against Hep G2 hepatocyte carcinoma cells and compound 4C against WI-38 normal cell line (red square). Percent inhibition was calculated as OD treated/OD control × 100%. The concentration-percent inhibition curve was used to calculate the concentration which caused 50% growth inhibition (IC50) by linear interpolation from a semi-log plot of a dose-response curve. **Figure S2.** The MTT assay results of the 11 tested compounds against A549 lung cancer cell line. Percent inhibition was calculated as OD treated/OD control × 100%. The concentration-percent inhibition curve was used to calculate the concentration which caused 50% growth inhibition (IC50) by linear interpolation from a semi-log plot of a dose-response curve. **Table S1.** Validation of the 3D-QSAR model. **Table S2.** Comparison between the experimental and predicted anticancer activity of the training set compounds against VEGFR-2 obtained by QSAR model.

Copyright notice: This dataset is made available under the Open Database License (http://opendatacommons.org/licenses/odbl/1.0). The Open Database License (ODbL) is a license agreement intended to allow users to freely share, modify, and use this Dataset while maintaining this same freedom for others, provided that the original source and author(s) are credited.

Link: https://doi.org/10.3897/pharmacia.69.e86504.suppl1